UNIVERSITY OF SOUTHAMPTON, 2012

FACULTY OF ENGINEERING AND THE ENVIRONMENT

SCHOOL OF ENGINEERING SCIENCES

The Effect of Leading Edge Serrations on Dynamic Stall

By: Jonathan Borg

A dissertation submitted in partial fulfilment of the degree of

MSc Aerodynamics and Computation by taught course.

The Effect of Leading Edge Serrations on Dynamic Stall

By Jonathan Borg

A dissertation submitted in partial fulfilment of the degree of

MSc Aerodynamics and Computation by taught course.

Abstract

An investigation into the effects of dynamic stall was carried out on six aerofoil profiles with sinusoidal leading edges having two amplitudes and three different wavelengths. The study also investigated the effect of spacing on the static performance of the aerofoil as well as the static hysteresis performance of these profiles. Compared to a baseline model it was found that a reduction in wavelength increased the maximum lift and the static stall angle. The maximum baseline lift was not reached in any of the cases. The static hysteresis performance of the sinusoidal leading edge profiles was found to be significantly better than the baseline with virtually no static hysteresis recorded. The dynamic study revealed that the sinusoidal profiles improved the performance of the aerofoil by increasing the maximum percentage of lift generated as well as by reducing the size of the hysteresis loop.

Preface

I would like to thank all those who supported me during my time here at the University of Southampton. My Supervisor, Dr. Bharathram Ganapathisubramani has been a constant source of inspiration and support. His invaluable advice and encouragement gave me the will power to perform to the best of my abilities. I would also like to thank Mr. Rammah Shami for his constant encouragement and help at times of need. Thanks also go to the staff at EDMC who fabricated all of my parts in a precise and timely manner.

I would like to thank my mum, dad and aunt for their financial and emotional support throughout this year and finally I would like to thank my girlfriend for being my rock and standing by me in difficult times.

Contents

Nomenclature

A: Amplitude

AoA: Angle of attack

$\bar{c}$: mean chord

C_d: Drag Coefficient

C_l: Lift Coefficient

k: Reduced Frequency

Re: Reynolds Number

U_∞: Free Stream Velocity

ω: Circular Frequency

ν: Kinematic Viscosity

λ: Wavelength

List of Figures

List of Tables

Chapter 1. Literature Study

1.1. Introduction

The phenomenon of dynamic stall has long been known to be a limiting factor in the performance of rotating blade machinery such as in helicopter blades and wind turbines. The unsteady loading is a common occurrence in helicopters in forward flight or in manoeuvres as well as in horizontal axis wind turbines when subject to a yaw error. This time-dependent loading causes aeroelastic problems which may influence the structural integrity and lifetime of these machines. [1]

Much research has been carried out into the study of dynamic stall and a sound understanding of the aerodynamic properties of this phenomenon has been achieved. This has served to stimulate further research which aims at reducing the detrimental properties of dynamic stall and hence improve the performance, reliability and cost of many existing machinery.

One such area of research is the field of biomimetics whereby inspiration to tackle engineering problems is drawn from biological organisms which are known to function or posses the same characteristics as the problem being addressed [2][3]. An attempt has been made to apply this ideology to address dynamic stall by drawing inspiration from the leading edge tubercles found on the fins of a Humpback whale. Previous research conducted on aerofoils with serrated leading edges has been carried out under static conditions and shall be discussed in further detail in Chapter 1 however, this study was the first attempt at investigating the effects of leading edge serrations on dynamic stall.

The main objective of this project was to investigate whether such leading edge serrations had any effect on the dynamic stall hysteresis loop, and if so, how the geometry influences the aerodynamic behaviour of the aerofoil. The project also aims to address the issue of the spacing between serrations on the generation of lift and drag under static conditions, as well as to investigate the effect of a sinusoidal leading edge on the static hysteresis performance of the aerofoil.

The report is divided into several chapters. Chapter 1 discusses some background information relating to biomimetics and the previous work that has been conducted on leading edge serrations thus far, elaborating on the results and aerodynamics of the leading edge serrations. A discussion on dynamic stall is also presented in this section whereby the mechanism driving the hysteresis loop and the properties influencing it are detailed. Chapter 2 gives an overview of the design of the experiment, the setup up and the experiments carried out to achieve the required objectives. These are followed by Chapter 3 and Chapter 4 which present the results for the static and dynamic experiments respectively. Some conclusions and remarks are then presented in Chapter 5.

1.2. Biomimetics: The Humpback Whale (Megaptera novaeangliae)

Figure 1: Humpback Whale (Source [4])

The field of biomimetics is an ever growing approach whereby engineers look upon nature's proven adaptation to particular environments for inspiration to solving engineering problems. The goal of such research is to emulate living organisms which possess similar characteristics or functions as the engineered system, and whose performance surpasses current mechanical technology, or provides new directions to solving existing problems. [3]

One such case of biomimetics is in the application of leading edge serrations to aerofoils. The inspiration of which was drawn from the leading edge tubercles found on the humpback whales' pectoral fins. The Humpback whale is a large mammal capable of growing to lengths of up to 13.5m and weigh up to 32,000 kg on average. Despite their large size, humpback whales are reported to be the most acrobatic of the whale species, capable of sharp, high speed banked turns which are used commonly as part of their feeding techniques. [5]

When performing 'bubble netting', the whales blow rings of bubbles which get successively smaller around their prey. These bubble rings range between 50m to 1.5m in diameter [5]. Upon completion of the net, the whales pivot sharply towards the centre of the net ascending to feed on the trapped fish. Another feeding manoeuvre which is commonly used by the humpback whale is to rapidly swim away from its prey, perform a 180 degree roll and lunge back towards its prey. The manoeuvre can be executed in 1-2 body lengths.

The manoeuvrability shown by the whale despite its large size has been attributed to the size and shape of its pectoral fins. Apart from having the largest fins compared to other whale species, the pectoral fins exhibit unique leading edge protuberances which are thought to influence the flow over the fin such that the lift and drag properties are enhanced. An investigation into the shape and size of a beached whale's fin revealed a symmetric profile which compared well to a symmetrical engineering aerofoil, namely the NACA 63_4021. It was also noted that the size and distance between the tubercles decreased with span-wise location.

Further studies were thus carried out to determine the influence that such protuberances had on aerofoil performance.

1.3. Static Studies on Serrated Leading Edges

The initial study of the beached whale revealed a lack of barnacles in areas between protuberances, which led to the hypothesis that the protuberance acted as vortex generators, channelling the high speed flow between peaks thus preventing barnacles from attaching to the fins. [6] Subsequent studies were thus conducted to understand the flow properties over the fin and determine the effect that such protuberances have on its aerodynamic behaviour.

The first study on a sinusoidal leading edge aerofoil conducted by Miklosovic *et al* [7] indicated an overall increase in performance at most points within the operational envelope. The research was conducted on an idealised scale model of a Humpback fin with a sinusoidal leading edge whose amplitude and peak spacing decreased with span-wise direction. A NACA 0020 profile was used for the model. The experiments were conducted in a closed circuit wind tunnel at a Reynolds Number of 5.05×10^5. (Where $Re = \bar{c}U/\nu^{-1}$ based on mean chord and free stream velocity). The results, compared to a similar model with a smooth leading edge, showed a 40% increase in stall angle and an increase of 6% in Cl_{stall} without any compromise to drag. In all of the cited studies however, this was the only investigation that obtained such positive results. A later study by Miklosovic *et al* [8] on a full span wing with a sinusoidal leading edge at a Reynolds number of 270,000 indicated a reduction in the maximum lift coefficient and stall angle. Comparing the two studies it was concluded that there exists a strong dependence on 3D effects with benefits that are a function of planform shape and Reynolds number.

Johari *et al* [9] investigated straight aerofoil sections having a NACA 63_4021 profiles with constant sinusoidal leading edge geometries having amplitudes of 2.5%, 5% and 12% of the mean chord length, with wavelengths of 25% and 50% of the mean chord length each. The plan-form area for all airfoils was kept constant and equal to the baseline airfoil having a straight leading edge. The experiments were carried out at a Reynolds number of 1.83×10^5. The results showed a decrease in the maximum lift coefficient as well as stall angle with increasing amplitude. In the post-stall region, the aerofoils with protuberances exhibited an increase in lift by as much as 50% over the baseline aerofoil. These aerofoils also had greater drag coefficients in the pre-stall region; however the drag was nearly independent of leading edge geometry in the post-stall region. A significant dependence on the amplitude of the leading edge geometry was determined whilst noting that the wavelength had only a minor effect on the results. The shorter wavelength aerofoil was found to exhibit marginally higher lift and marginally lower drag compared with the longer wavelength aerofoils.

Apart from the decrease in maximum lift coefficient and stall angle, the amplitude was also found to effect the stall behaviour of the aerofoils such that softer stall was obtained with increasing amplitudes. At the largest amplitude, the aerofoil did not stall in a traditional way but rather maintained a near constant maximum lift coefficient.

The effect of amplitude on the performance of the aerofoils was corroborated by the results of Hansen *et al* [10] who investigated the three-dimensional effects on the performance of aerofoils having a sinusoidal leading edge. It was found that there was no significant difference between the 2-Dimensional and 3-Dimensional cases, suggesting that the protuberances act as wing fences which restricted span-wise flow. The drag performance of the aerofoils was such that an increase in drag was exhibited in pre-stall regions followed by a decrease in drag in post-stall regions compared to the baseline aerofoil for all aerofoils tested. A dependence on wavelength was also determined, such that a reduction in spacing between successive peaks improved the performance of the aerofoil up till a minimum value. Beyond this point, a reduction in performance was observed, resulting in a lower maximum lift coefficient and a lower stall angle. It was concluded from this research that aerofoils with a sinusoidal leading edge do not effect significantly the formation of wing tip vortices and that the best configuration was the one having the smallest amplitude and smallest wavelength.

A further study by Hansen *et al* [11] suggested that the influence of leading edge tubercles is very much related to the profile being investigated. Two profiles having different locations for maximum camber were used in this study. It was found that the aerofoil having the maximum camber at a 50% location of the chord experienced a minimal reduction in performance in pre-stall regions compared to an aerofoil with a maximum camber at 30% location of the chord. Thus aerofoils having a maximum camber which is further aft benefit more from a sinusoidal leading edge.

1.4. Aerodynamics of Sinusoidal Leading Edge Aerofoils

In traditional aerofoils, stall is known to occur in one of two ways depending on the thickness of the aerofoil. A thin aerofoil will undergo leading edge stall, where the flow separates quite suddenly from the leading edge and over the top surface of the aerofoil. Thick aerofoils on the other hand experience trailing edge stall where a gradual movement of separation from the trailing edge toward the leading edge results with an increase in the angle of attack. The aerofoil stalls when separation reaches the leading edge. Leading edge stall is more abrupt however such aerofoils tend to generated more lift than thick aerofoils.[12]

Stall in aerofoils with serrated leading edges however is not as straight forward. The various studies which have investigated how such aerofoils stall and how the aerodynamics behave have led to a division of opinion.

In his aerodynamic model, Neirop *et al* [13] proposes that the bumps on the leading edge alter the pressure distribution over the aerofoil such that separation of the boundary layer behind the bumps is delayed. His study suggests that since neighbouring bumps and troughs have similar thicknesses but different chord lengths, the same pressure distribution must be overcome over a shorter distance behind a trough. This leads to a greater adverse pressure gradient which causes separation to occur behind troughs. A flow visualisation exercise by Johari [9] validates such an observation. In line with experimental results the model predicts a smoother transition to stall. Also, since stall occurs earlier in troughs, a significant part of the aerofoil will be in stall at smaller angles of attack hence the maximum lift is not achieved. The model however shows minimal dependence on the separation between peaks and predicts an increase in stall angle which was not observed in subsequent experimental results.

In contrast to Neirop's hypothesis, other researchers argue that the peaks function as vortex generators, providing momentum to the flow between peaks hence delaying stall in these regions. PIV tests conducted by Stanway [14] on a hydrofoil resembling a humpback whale's fin having a NACA 0020 profile showed the formation of highly organized vortical structures forming between peaks at an angle of attack of 10^0. The vortical structures appear as two contra-rotating vortices whose strength increases with increasing angles of attack. The vortices act in a manner similar to leading-edge vortices of a delta wing, with the suction force of the vortex producing lift at high angles of attack. Also, minimal span-wise flow was observed which validate the results by Hansen *et al*.

One can however also argue that the mechanism driving stall delay is a combination of the two arguments presented above. Based on Neirop's hypothesis, the larger pressure gradient that is required to be overcome by the flow over the troughs leads to early separation, thus resulting in a reduction in the maximum lift obtained. Upon further increase in angle of attack however, the vortices generated by the peaks increase in strength maintaining lift to higher angles of attack. However, since vortex generated lift is not as strong as pressure generated lift, maximum lift cannot be achieved.

1.5. Dynamic Stall

The dynamic stall phenomenon has long been recognized as a limiting factor in rotating blade machinery undergoing time-dependent unsteady motion. Rotating blade machinery such as helicopter blades and wind turbines experience rapid changes in the angle of attack of the blades, resulting in flow separation and stall in a dynamic time-dependent manner, hence referred to as dynamic stall [1]. The rapid oscillations of the aerofoil result in a delay in stall to incidences considerable larger than that of a static stall angle. Once dynamic stall does occur however, it is much more severe than in static stall and results in the formation of a hysteresis loop which is detrimental to the fatigue of the blade. [15]

The dynamic stall phenomenon has been studied in detail both experimentally and analytically such that the flow pattern over a lifting surface in dynamic stall is well understood. Referring to Figure 2 below:

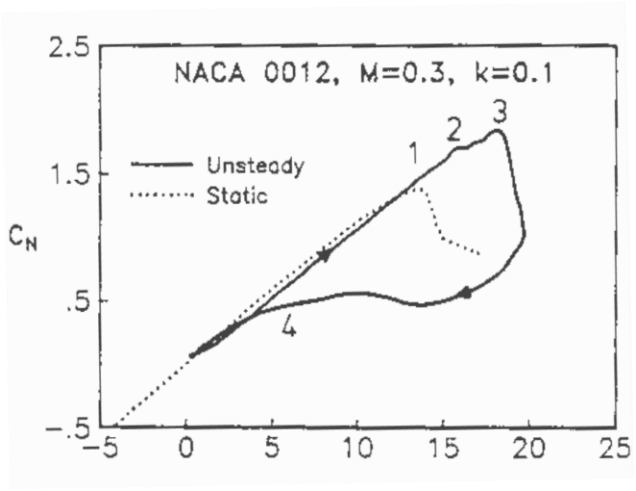

Figure 2: Dynamic Stall Hysteresis Curve. Source [16]

In the unseparated region up till point 1 the lift curve follows the same trend as in the static case with no significant change to the flow properties. At point 1, the aerofoil exceeds the static stall angle and flow reversal takes place in the boundary layer, starting from the trailing edge and moving successively closer to the leading edge. At point 2 the vortex detaches and between points 2 and 3, the vortex sweeps over the aerofoil surface inducing extra lift and aft centre of pressure movement. The peak in lift at point 3 is the point at which the vortex reaches the trailing edge of the surface thus resulting in an extensive loss of lift. Flow reattaches at point 4 when the angle of attack becomes low enough for the flow to reattach from the front to the back. [15, 16, 17]

The instantaneous angle of attack for an aerofoil undergoing dynamic stall is defined by:

$$\alpha(t) = \alpha_0 + \alpha_m \sin(\omega t) \dots (1)$$

McCroskey [15], Brydges [17] and Leishman [18] noted that the extent of dynamic stall is characterised by three main parameters namely; reduced frequency k, amplitude of oscillations α_m and the mean angle of oscillations α_0. Where the reduced frequency k is defined by

$$k = \frac{\omega \bar{c}}{2U_\infty} \dots (2)$$

The effect of increasing the reduced frequency was found to delay the onset of separation and dynamic stall to higher angles of attack. Similarly to the effect of reduced frequency, the amplitude of oscillation also affects the onset of dynamic stall, with large amplitudes resulting in large primary peaks in lift followed by strong secondary peaks on the down-stroke motion of the aerofoil. The mean angle of attack on the other hand influences the extent to which dynamic stall occurs. If the mean angle of attack is low enough, the flow may remain attached over the lifting surface and dynamic stall will not occur. Increasing the angle of attack causes the aerofoil to undergo light stall until the mean angle is high enough to undergo deep dynamic stall, resulting in a large hysteresis loop.

1.6. Dynamic Studies on Serrated Leading Edges

Ever since the dynamic stall phenomenon was realized, many studies were focussed on understanding the flow physics and finding ways by which the hysteresis loop could be reduced. One of the objectives of this project was to attempt to apply the biomimetic approach of using a sinusoidal leading edge aerofoil and subjecting it to dynamic stall to determine the influence of the leading edge geometry on the hysteresis loop. To the author's knowledge, there has been no such work carried out on these aerofoils.

Previous dynamic testing by Stanway [14] and Ozen and Rockwell [19] was carried out on flapping foils. Stanway conducted his experiments to determine the influence of leading edge tubercles on hydrodynamic forces. His results showed that the introduction of leading edge tubercles on the control surface degraded its performance which resulted in a reduction in thrust and efficiency. Ozen and Rockwell's tests showed a significant reduction of span-wise flow for a flapping flat plate with a sinusoidal leading edge as opposed to one with a straight edge.

Dynamic stall tests have also been carried out on aerofoils with leading edge vortex generators by Hein *et al* [20]. The tests showed promising results with an improved performance under dynamic conditions which resulted in a reduction in the hysteresis loop. While parallels can be drawn to this test, the leading edge used in these experiments was uniform along the span and not sinusoidal. There have been no experiments conducted to date which have examined the effect of amplitude and wavelength of a sinusoidal leading edge on dynamic stall.

1.7. Research Objectives

Following the literature survey, several key discrepancies were noted in previous work which this study aims at investigating.

- The first objective is the investigation into the effect of peak spacing on the lift and drag characteristics under static conditions. Whereas the effect of amplitude has been corroborated by various studies, there is no conclusive evidence on what the effect of peak spacing is.
- The second objective of this study is to investigate the effect of the sinusoidal leading edge geometry on the static hysteresis performance.
- The third and final objective of this project is to determine the effect of the leading edge geometry on the dynamic stall characteristics of the aerofoil.

A significant portion of the project was thus dedicated to designing an experiment which would enable the study of both the static and dynamic requirements of the project.

Chapter 2. Experimental Setup

2.1. Wind Tunnel

The wind tunnel used to carry out the experiments was the Lancaster wind tunnel at the University of Southampton. It is an open circuit, closed jet wind tunnel having a 0.6x0.9x4.5m test section and a contraction nozzle equipped with flow straighteners and a honey comb mesh to reduce turbulence. The flow is driven by a 50Hp motor and can provide wind speeds of up to 40m/s. Wind speed was measured through a pitot tube connected to a digital manometer which provides instantaneous wind speeds in m/s to an accuracy of 0.2 m/s.

2.2. Aerofoil Design and Test Parameters

To carry out a thorough investigation of both the static and dynamic aspects of this project, several key geometrical and operational decisions were required to be taken to enable the correct design and selection of the key components driving the system.

2.2.1. Geometry

To investigate the effects of wavelength 6 aerofoils were designed having two different amplitudes and three different wavelengths, together with a baseline aerofoil for comparison. Two non-dimensional parameters, A/c and λ/c were used to define the leading edge geometry with respect to the mean chord, where A and λ were defined as shown in Figure 3 below. The profiles were designed such that the total planform area was constant for all aerofoils.

The overall dimensions of the aerofoils were designed such that the blockage in the test section was less than 5% at a maximum pitch of 30^0. Hence a mean chord and span of 0.1 and 0.25m respectively were used.

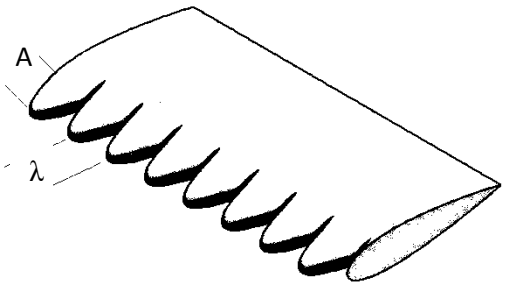

Figure 3: Aerofoil Parameters

The profile of choice for the aerofoils was the NACA 0021 profile. This was chosen since it is similar to the profile found on the humpback whale's flippers and was used in previous studies, thus allowing for some comparisons to be made. The NACA 0021 profile is also used in wind turbine blades.

The geometric parameters for the static stall experiments are summarized in Table 1 below

Profile	NACA 0021	
Mean Chord	0.1m	
Span	0.25m	
Leading Edge Geometries		
A/c	**λ/c**	**Label**
0	0	**Baseline**
0.05	0.25	**A1F3**
0.05	0.33	**A1F2**
0.05	0.5	**A1F1**
0.12	0.25	**A2F3**
0.12	0.33	**A2F2**
.12	0.5	**A2F1**

Table 1: Geometrical Properties of Aerofoils

2.2.2. Operational Requirements

Keeping the research in line with previous studies, the tests were to be run at a Reynolds number of 130,000 therefore, based on the chord of the aerofoils, the tests were to be conducted at a flow speed of 19m/s.

A reduced frequency of 0.08, requiring oscillations at 5Hz were to be generated for the dynamic experiments. Two mean amplitudes were to be tested for each of the aerofoils; the first at 3 degrees lower than the static stall angle, and the second at an angle of 5 degrees higher than the static stall angle. The later was selected since, under static conditions, the main benefit of these aerofoils lies in the post stall region. Hence, it was decided to investigate the dynamic characteristics of the aerofoils under high angles of attack. The dynamic experiments were to be carried out at amplitudes of 5^0 and 7^0.

2.3. Manufacture of Aerofoils

Three dimensional drawings of the aerofoils were designed using Autodesk Inventor and exported to be 3D printed using a ZCorp 650 3D printer. The printer uses a high performance composite powder and prints to an accuracy of 0.2mm. Since the resulting greens were very brittle after printing, an infiltration process was then required to strengthen the model. This involved spraying the models with a resin to bind the powder together and form a durable model.

The resulting surface of the model had a relatively high roughness after the printing process was complete and some post-processing was required to achieve a smooth finish. Due to the high cost of printing, the aerofoils were designed such that the trailing edge was common to all the leading edges, thus minimizing the material used. Figure 4 below shows the six aerofoil profiles together with the baseline profile and the common trailing edge. Figure 5 shows the complete aerofoil having the A2F3 leading edge.

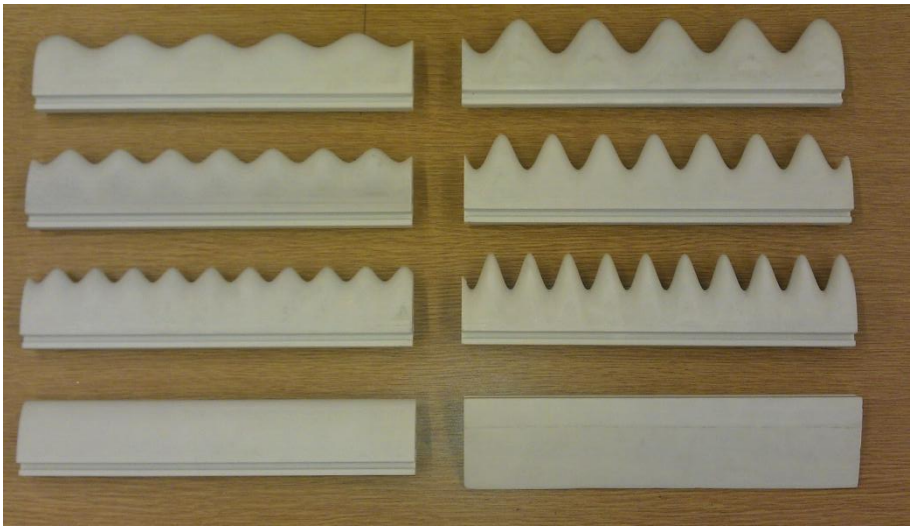

Figure 4: Six Leading Edges together with Baseline and trailing edge.
[Left-Top to Bottom- A1F1, A1F2, A1F3, Baseline], [Right-Top to Bottom- A2F1, A2F2, A2F3, Trailing Edge]

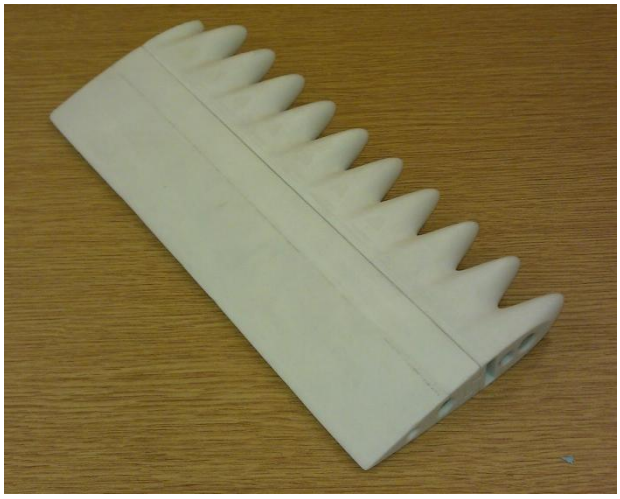

Figure 5: A2F3 Aerofoil

2.4. Shaft Design and Motor selection

The experimental setup shown below in Figure 6 was designed such that the aerofoil stood vertically in the wind tunnel, thus reducing gravitational effects. A shaft through the quarter chord of the aerofoil connected it directly to a servomotor through the use of a coupling. The servomotor system would control both the position of the aerofoil as well as provide the oscillations required for dynamic stall. Strain gauges fixed manually to the base of the shaft were used to measure the strain and hence determine the forces acting on the aerofoil. A stiff aluminium frame to house the motor was also designed to complete the system.

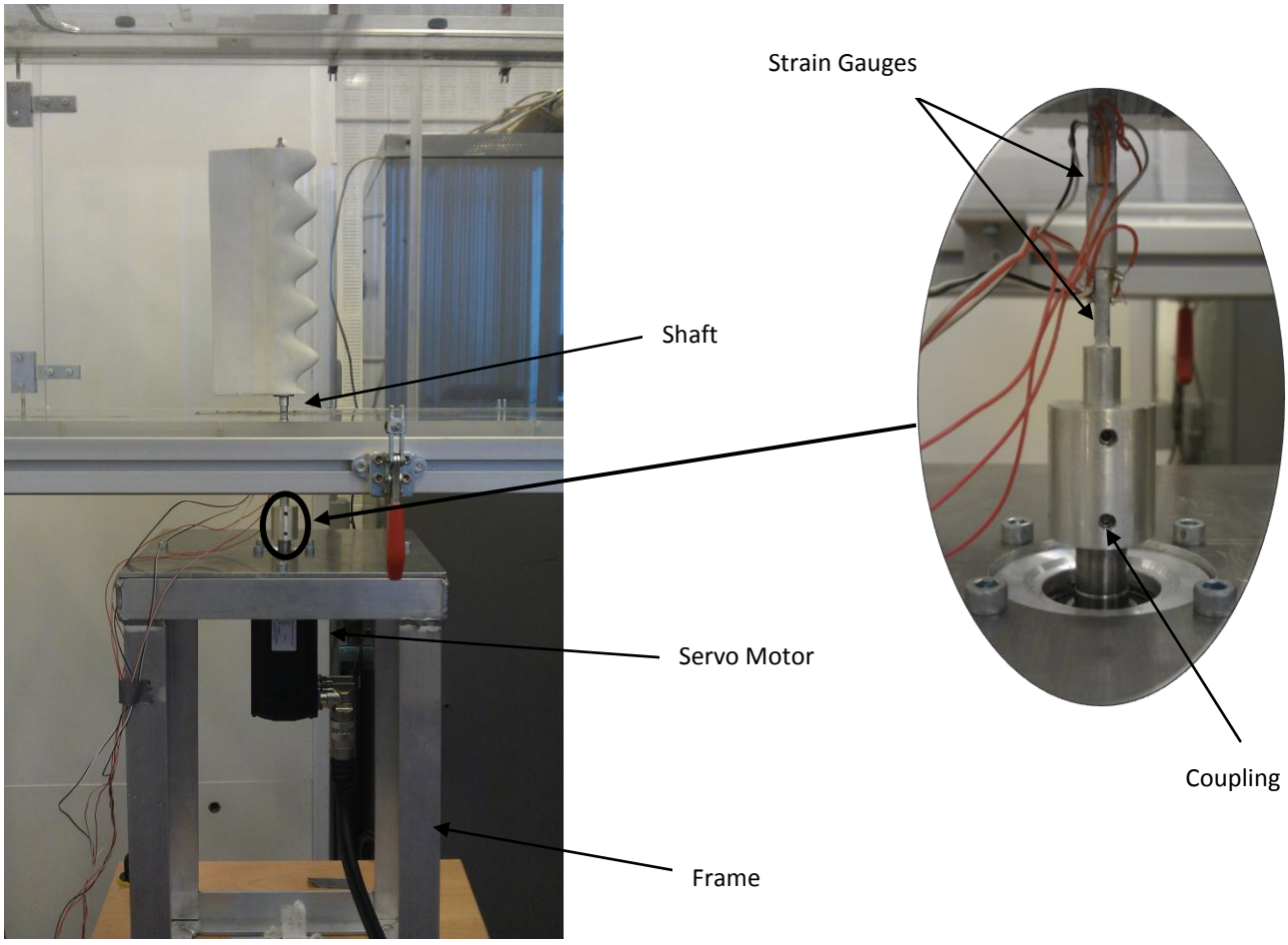

Figure 6: Equipment Setup

Preliminary calculations of the expected loads were carried out to ensure that the strain experienced by the shaft was measurable. It was thus assumed that the lift and drag forces acted as uniformly distributed loads along the span of the aerofoil. Using a bending moment diagram for the lowest measure of force, the moment at the base was calculated. Hence the maximum thickness of the shaft that would enable the measurement of such strain was determined. The 120 ohm strain gauges were applied manually to the shaft and connected in a half-bridge Wheatstone configuration to an NI 9237 data acquisition card connected to an NI CompactRio 9074 chassis.

Following the design of the shaft and aerofoil, a servo motor system capable of producing the required torque and speed was selected. The selection process involved the calculation of the moment of inertia of all the components being driven by the motor and hence the torque required to sustain the oscillations. The shaft and coupling were manufactured from high strength aluminium in order to reduce the weight and moment of inertia of the system.

An AKM33E servomotor with a built-in encoder, detailed below, together with a Kollmorgen AKD driver was used to drive the system. Control was provided by an NI 9514 controller which was also connected to the CompactRio Chassis. This system allowed the simultaneous control of both the strain data acquisition as well as the control of the motor due to an internal clock in the chassis which synchronized all events. The data flow diagram for the system can be found in Appendix C.

Motor Details	
Type	Brushless
Continuous Torque at Stall (Nm)	2.79
Peak Torque at Stall (Nm)	9.96
Rotor Inertia (Jm) kg-cm2	0.045
Encoder Details	
Resolution	2^{24} counts per revolution
Accuracy	±16 arc-min net (0.26 deg)

Table 2: Motor Specifications

2.5. Motor control: LabView Program

The positioning, dynamic motion and strain gauge data acquisition were controlled via a custom built program using National Instruments LabView software. The purpose of the program was to enable the simultaneous control of both the position of the aerofoil as well as the collection of the strain gauge data in a single user interface. The program was therefore programmed to fulfil the following functions.

- Control the angular position of the aerofoil in one degree increments with the possibility of 0.5 degree increments
- Display strain and position data in real time to enable quick identification of any problems in the system
- Trigger static data acquisition at the push of a button
- Record data for a finite period of time
- Provide sinusoidal oscillations at a specific frequency
- Provide control over the amplitude of oscillations
- Maintain axis position when switching between static and dynamic operation thus enabling the user to set the mean angle of attack about which oscillations take place
- Trigger dynamic data acquisition at the push of a button
- Record the simultaneous position and strain gauge data
- Abort dynamic motion in case of system malfunction
- Prompt user of any system errors
- Save data to file

The program was built around a system of case structures which could be accessed by means of a menu. This ensured a logical progression between the static and dynamic controls thus avoiding any potential damage to the system. Each structure contained one high priority loop and one low priority loop. The purpose of the high priority loop was to control all the hardware functions such as the control of the motor and the acquisition of strain data. This loop was timed and synchronized to the CompactRio scan engine to ensure each item within the loop was executed on time. The acquired data, including the position of the motor, the strain from each half bridge and the timestamp, were then saved to local variables. These variables were then accessed at the low priority loop to display and save the data to file.

2.6. Experimental campaign

The experimental campaign was split into two main tasks; the static study of the aerofoils and the dynamic stall experiments. The following section will present the procedure adopted to perform both sets of experiments as well as the calibration of the instrumentation and the data analysis required to achieve the results.

2.6.1. Static Study

The purpose of the static study was to address two fundamental issues relating to a sinusoidal leading edge profile. The first objective was to shed further light onto the effect of wavelength of the leading edge geometry on the lift and drag performance of the aerofoil and determine whether a decrease in amplitude spacing has any significant effect on the maximum lift and stall angle characteristics.

The second objective was to investigate and document the static hysteresis performance of each aerofoil compared to the baseline aerofoil. This study is aimed at determining whether an aerofoil with a sinusoidal leading edge exhibits the same static hysteresis loop observed in a traditional aerofoil.

2.6.1.1. Calibration

The strain gauges were calibrated before the experiments were initiated by adopting the procedure described below.

Calibration was performed with the aerofoil in place since the shaft did not pass through the centre of gravity of the aerofoil, hence causing a moment which would have resulted in some error in the final results. Calibration was performed by loading the aerofoil at a known distance from the strain gauges by calibration weights suspended from a string which was passed through a pulley. The pulley was suspended from a shaft at the centreline of the wind tunnel at a distance of 0.2m from the aerofoil's axis of rotation. Prior to calibration, it was ensured that upon loading there was minimal cross-talk between the half-bridges by rotating the aerofoil until the optimal position was reached. The system was then loaded with 50gr weights over a range from 0 to 350gr. Two calibration curves, one for each half bridge were conducted at 0^0 and 90^0, representing the tangential and normal forces respectively.

Due to a minor fabrication error between the machined surfaces of the strain gauges at the base of the shaft and the machined surface holding the aerofoil along its span, the 0^0 angular position of the aerofoil with respect to the wind tunnel did not coincide with the 0^0 angular position identified to eliminate cross-talk between the two strain gauge bridges. To find the true zero position of the aerofoil with respect to the flow, experiments were conducted by varying the attack angle of the foil by half-degree increments within the initial linear lift range of the C_l curve between $-4^0 < \alpha < 4^0$ until zero lift was recorded. The lift curve was assumed to be symmetric about $\alpha = 0$ since the aerofoil was symmetric and uncambered.

2.6.1.2. Experimental Procedure

Once calibration was complete several data acquisition runs were performed with the wind tunnel speed set to 19 m/s. The first run acquired data over a range of angles between $-1^0 < \alpha < 21^0$ at one degree increments. A second run was performed at the same conditions to ensure short term reliability. The third and final run was conducted to test for static hysteresis. This involved pitching the aerofoil up to 21^0 then pitching it back down to -1^0 at one degree increments. At each angle the flow was left to settle for approximately ten seconds before data acquisition was started. Data was then gathered for 15 seconds for all the tests mentioned above. Once all the tests were completed the baseline aerofoil was retested to ensure medium term reliability. Both the short and medium term results were found to coincide with the original tests.

2.6.1.3. Data processing

The raw voltages acquired from the Wheatstone bridges were converted to the equivalent lift and drag coefficients through a series of data operations. The voltages acquired at each angle of attack were averaged over the duration of data acquisition time and converted to their equivalent normal and tangential forces using the calibration curves obtained earlier. The normal and tangential forces were then converted to lift and drag using simple trigonometric relationships between the forces as shown in Figure 7 below.

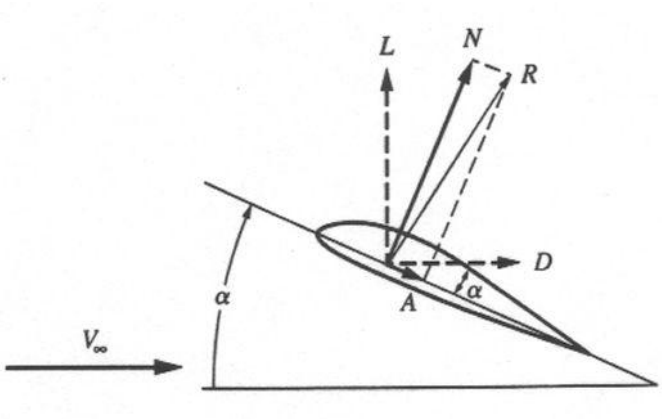

Figure 7: Forces on Aerofoil

Since the aerofoil was subject to a misalignment error the difference in angle was added to the angle of attack using

$$Drag = Acos(\alpha + \Delta\alpha) + Nsin(\alpha + \Delta\alpha)$$

$$Lift = Ncos(\alpha + \Delta\alpha) - Asin(\alpha + \Delta\alpha)$$

Knowing the lift and drag forces their respective coefficients were calculated using:

$$C_l = \frac{L}{\frac{1}{2}\rho AU^2} \quad C_d = \frac{D}{\frac{1}{2}\rho AU^2}$$

Chapter 3. Results: Static Stall

In this chapter, the results for the first two objectives related to the static investigations of the serrated leading edges are presented. The first section presents the overall aerodynamic performance of the aerofoils with different serrated leading edges whilst the second section presents the static hysteresis stall results.

3.1. Part 1: Aerodynamic Performance

The first part of the static analysis compares the lift and drag coefficients of the six aerofoils having a sinusoidal leading edge with the baseline aerofoil. Figure 8 and Figure 9 show the lift and drag curves for the aerofoils having the lowest amplitude with varying wavelengths whilst Figure 12 and Figure 13 show the lift and drag curves for the aerofoils having the large amplitude with varying wavelengths.

The principal features and trends exhibited by previous studies can be seen to have been reproduced in the results below. In general one can note from Figure 8 and Figure 12 that a decrease in the maximum lift coefficient was achieved for all profiles. This was also accompanied by a reduction in the static stall angle. Softer stall characteristics are evident with an increase in the geometrical amplitude as well as sustained lift at higher angles of attack. Similarly to previous studies an increase in drag was recorded in the pre-stall region of the drag curves.

3.1.1. Low Amplitude Aerofoil Analysis

3.1.1.1. Lift Analysis

A more detailed analysis of the results reveals that the baseline profile achieved a maximum lift coefficient of 0.9 at an angle of attack of approximately 16^0. This was followed by a maximum lift coefficient of 0.75, 0.67 and 0.61 for the sinusoidal profiles with progressively longer wavelengths. The stall AoA also increased from 11.5^0 for the longest wavelength to 13^0 for the shortest.

These results show a clear improvement for the lift coefficient in pre-stall regions, with the shortest wavelength exhibiting a lift coefficient of 0.14 higher that the largest wavelength for the smallest amplitude. In the post stall region of the lift curve an increase in performance of up to 80% can be seen for the lowest amplitude and lowest wavelength case. In the study conducted by Hansen using a NACA 0021 profile operating under similar conditions a performance increase of up to 61% was achieved.[10]

The dip in lift due to stall for the sinusoidal profiles is of 20%, 21.5%, 18.7% for the smallest, medium, and largest wavelengths respectively. The latter performs marginally better than the other two aerofoils, however the dip in lift due to stall seems to be independent of the wavelength. These results mark a significant improvement over the 60% reduction in lift for the baseline case.

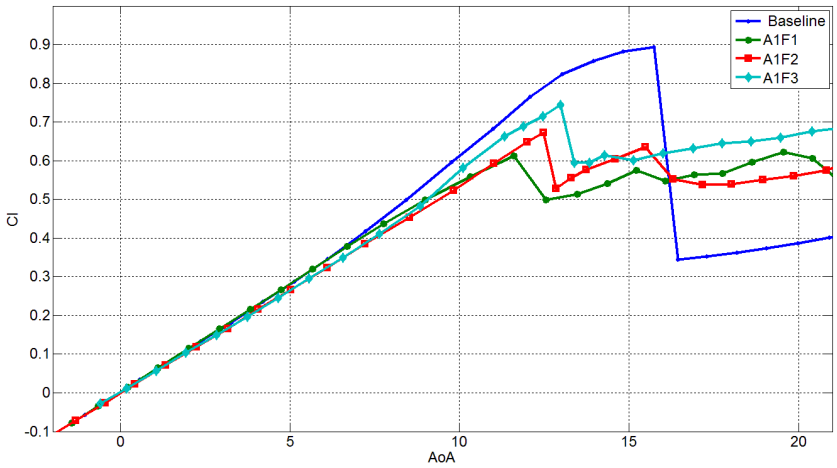

Figure 8: Static Lift Coefficient Vs AoA for Baseline and Low Amplitude Aerofoils

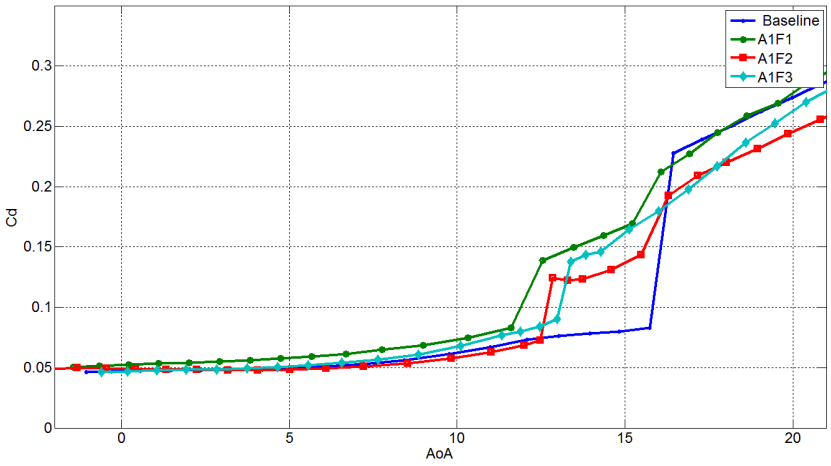

Figure 9: Static Drag Coefficient Vs AoA for Baseline and Low Amplitude Aerofoils

Figure 10 shows the percentage difference between the baseline aerofoil and the sinusoidal aerofoils. It can be seen that in the pre-stall region, the aerofoils experienced a reduction of up to 40% in lift however; this loss was recovered in the post stall region with an approximate 40% and 60% gain for the largest and medium wavelength aerofoils respectively at 20^0. The shortest wavelength performed better in both regions with a 35% reduction in lift in the pre-stall region and a 70% increase in lift at 20^0.

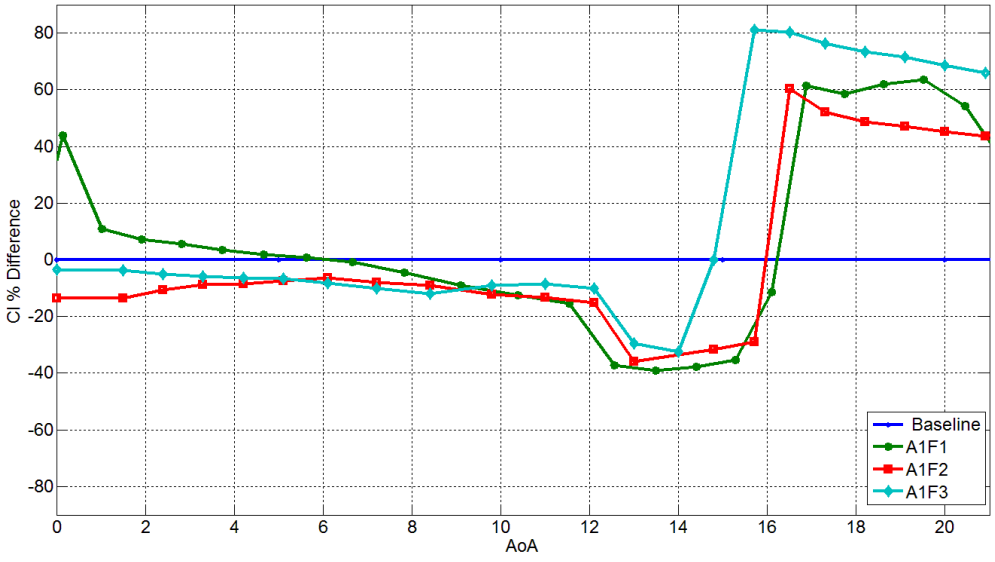

Figure 10: Percentage Difference in Lift Coefficient between the Low Amplitude sinusoidal aerofoils and baseline aerofoil as a function of AoA

3.1.1.2. Drag Analysis

The drag performance figure below shows a significant increase in drag in the pre-stall region. The aerofoil with the longest wavelength performs the worst of the three with an increase in drag of up to a 105%. In post stall however there was negligible difference. Contrary to the trend observed for lift, the aerofoil with the medium wavelength performed better than the aerofoil with the lowest wavelength. In the former, a maximum increase of 70% was noted, compared with a maximum of a 100% increase in drag for the shortest wavelength. Also, whilst both cases performed better than the baseline case in the post stall region, the aerofoil with the medium wavelength sustained a reduction in drag of up to 15% up till 21^0, whereas the other aerofoils tended towards the baseline drag.

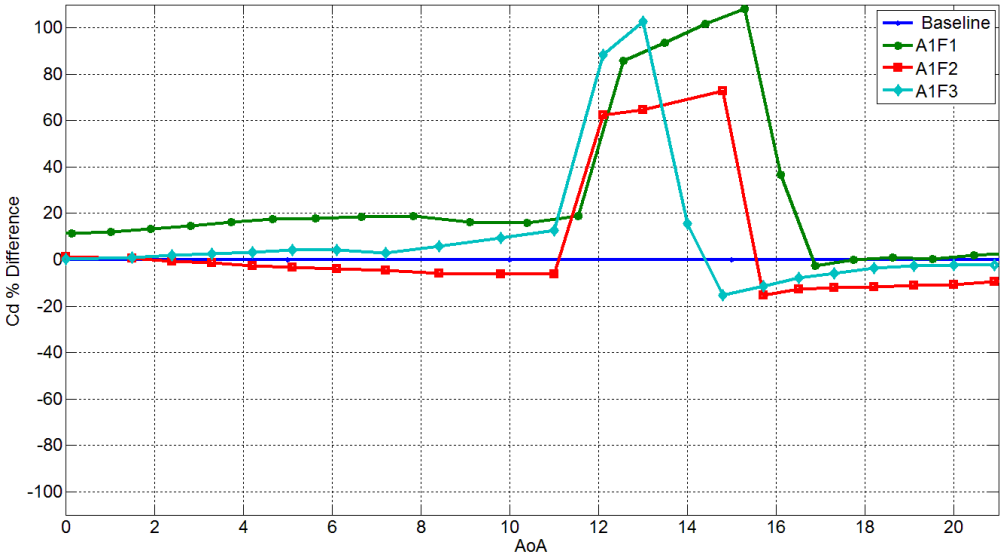

Figure 11: Percentage Difference in Drag Coefficient between the Low Amplitude sinusoidal aerofoils and baseline aerofoil as a function of AoA

3.1.2. High amplitude Aerofoils

3.1.2.1. Lift Analysis

When comparing the aerofoils with different geometrical amplitudes it becomes immediately apparent that, as previous studies have suggested, the amplitude has a significant effect on the lift characteristics of the aerofoil. An interesting feature in this set of results seen below in Figure 12 is the effect of wavelength at large amplitudes. Whereas at the lowest amplitude the performance increased with a reduction in wavelength, by using a large amplitude the performance improved from the largest to the medium aerofoil, then reduced at the lowest wavelength. This result was observed by Hansen *et al*, who noted that a limit in the reduction of wavelength existed, after which the performance of the aerofoil degraded [10]. Since this degradation in performance was noted at only one of the amplitudes, the result suggests that there exists a relationship between amplitude and wavelength and the two cannot be analysed independently.

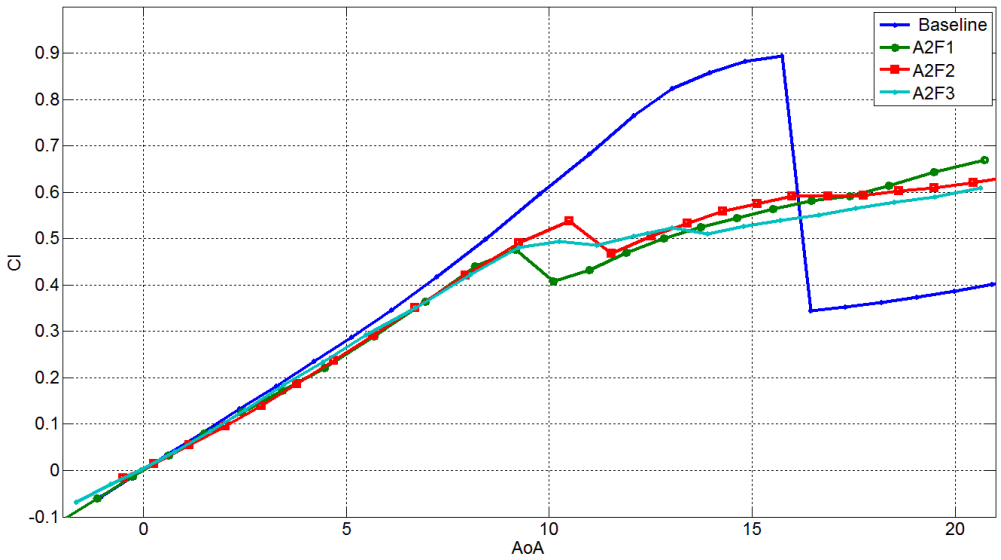

Figure 12: Static Lift Coefficient Vs AoA for Baseline and High Amplitude Aerofoils

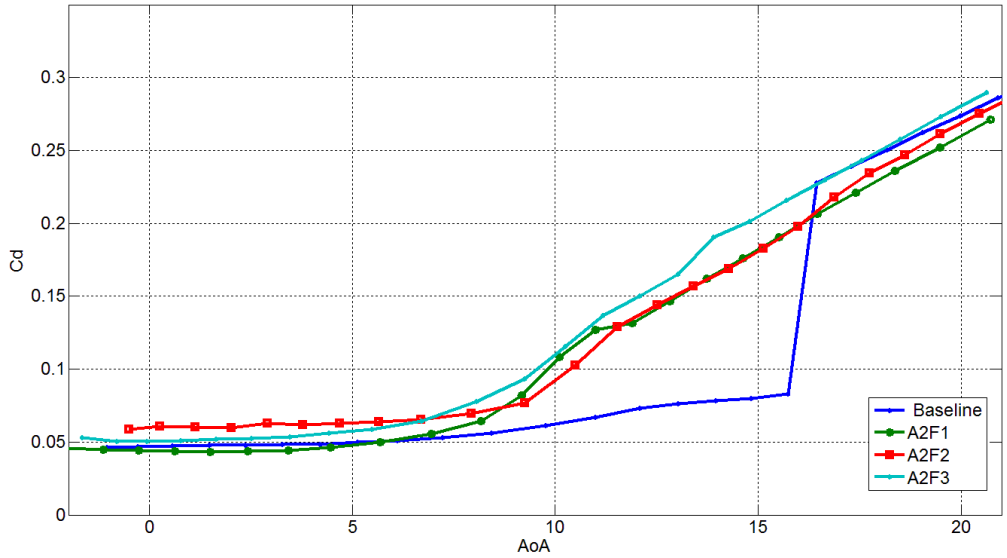

Figure 13: Static Drag Coefficient Vs AoA for Baseline and High Amplitude Aerofoils

Considering the aerofoils at the largest amplitude, one can note that the maximum lift generated by the aerofoils reduced by 47%, 40% and 44% for the largest, medium and smallest wavelengths, compared with a reduction of 32%,25% and 17% for the largest, medium and shortest wavelengths at the lowest amplitude. A marked improvement is achieved by using a lower amplitude as suggested by previous studies. The lower amplitude aerofoils also perform better over the whole range of angles of attack. Whilst the maximum reduction in lift is similar to the low amplitude aerofoils at 40%, the range over which this reduction occurs is between $11<\alpha<16$ compared to $13<\alpha<15$ at the lower amplitude. The gain in lift in the post stall regions is also lower, at a maximum of 60% for the aerofoil at the medium wavelength.

The stall characteristics of the large amplitude are however softer than the shorter amplitude aerofoils. At the largest and medium wavelengths the loss of lift is of 13% and 15% respectively whereas at the smallest wavelength, the aerofoil did not stall in the traditional way but rather maintained a near constant lift coefficient of approximately 0.5.

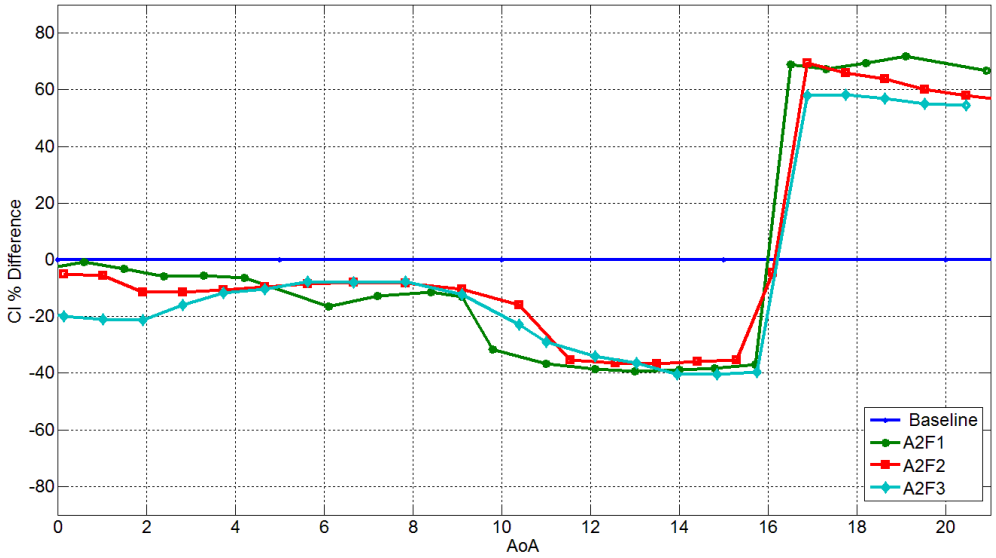

Figure 14: Percentage Difference in Lift Coefficient between the high Amplitude sinusoidal aerofoils and baseline aerofoil as a function of AoA

3.1.2.2. Drag Analysis

The results for the aerofoils' drag characteristics were as similar to those at the lower amplitude, with an increase in drag in the pre-stall region and a negligible difference in the post stall region. Compared to the results of the lower amplitude aerofoils however the performance was noted be worse, with a maximum increase in drag of 150%. Similarly to the lift characteristics of this set of aerofoils, the increase in drag was recorded over a larger range of angles of attack. Also, whereas the aerofoils with the smallest amplitude showed an improvement in performance in post stall, with less than 5% improvement in the drag coefficient, the effect can be considered to be negligible at this amplitude.

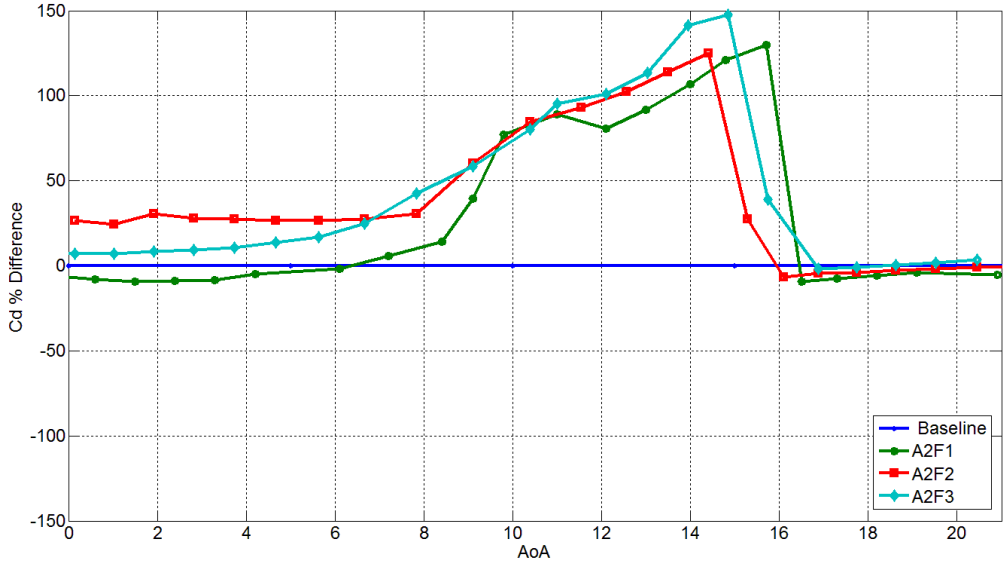

Figure 15: Percentage Difference in Drag Coefficient between the high Amplitude sinusoidal aerofoils and baseline aerofoil as a function of AoA

It is evident from the results of this study that the low amplitude, low wavelength aerofoil has better lift and drag characteristics than the other sinusoidal leading edge aerofoils.

3.2. Part 2: Static Stall Hysteresis

The second objective of the static analysis was to determine the effect of the sinusoidal leading edges on the static hysteresis performance of the aerofoils. Once the pitch of an aerofoil is increased beyond the static stall angle and stall occurs, the flow does not re-attach at the same angle once the pitch is lowered.

As shown in Figure 16 below, at approximately 11^0, the flow can be seen to re-attach at a significantly lower angle, resulting in a drastic reduction in performance over the range $11<\alpha<16$ when compared to the lift obtained before stall was reached. Figure 17 shows that static hysteresis also results in a significant increase in drag, thus resulting in a considerable overall loss in performance. This effect is particularly detrimental to a wing which is operating at high angles of attack close to the static stall angle with the possibility of exceeding it, since this would require the wing angle to be reduced to the re-attachment angle before any useful lift is generated.

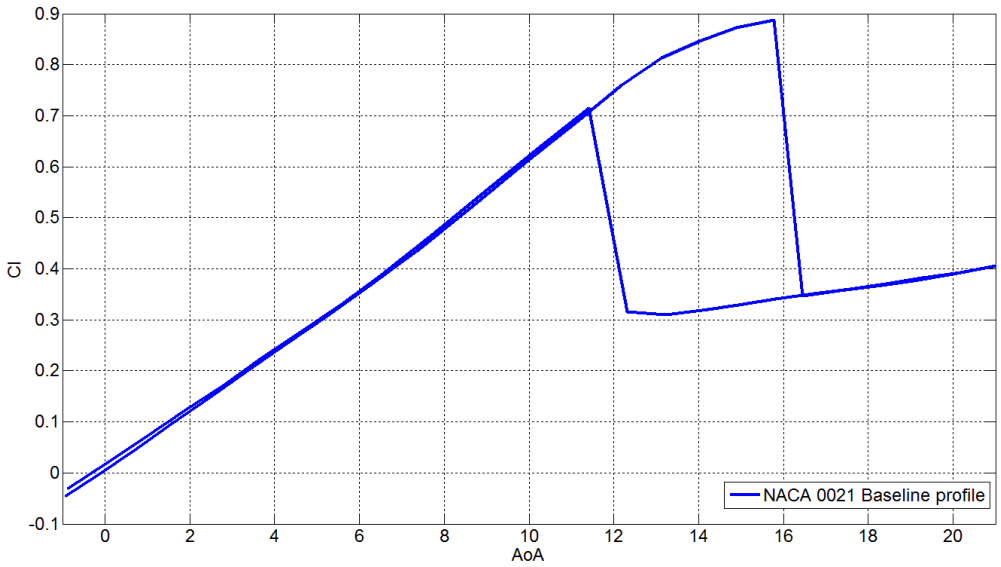

Figure 16: Baseline Static Lift Hysteresis

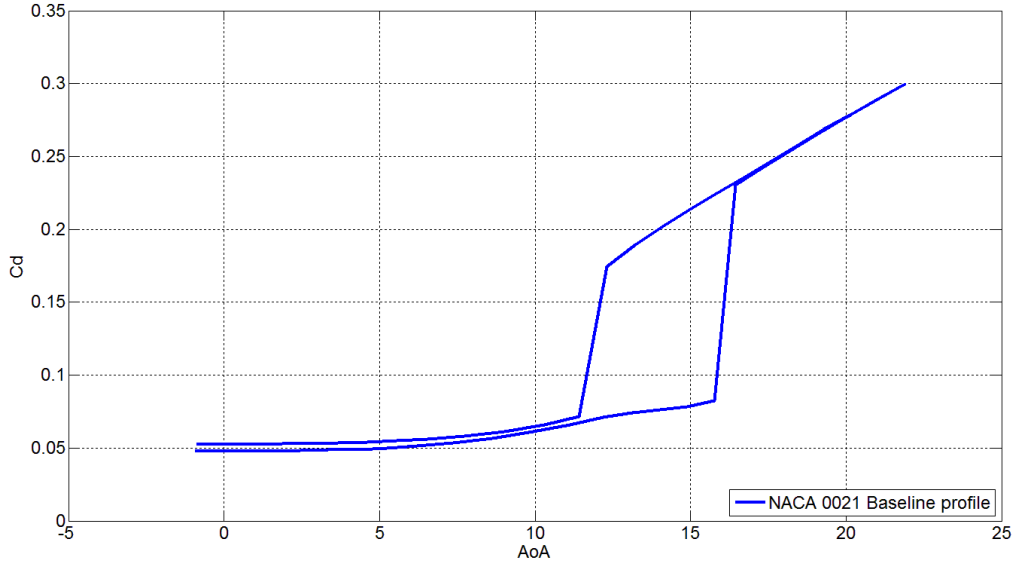

Figure 17: Baseline Static Drag Hysteresis

3.2.1. Sinusoidal Leading Edge Aerofoils Analysis

Similarly to the baseline aerofoil, the sinusoidal profiles were pitched to a maximum angle of 21^0 and pitched down in one degree increments to obtain their respective hysteresis curves. The percentage difference between the pitching up and pitching down lift and drag coefficients were then plotted in Figure 18 to Figure 21 below.

Figure 18 and Figure 19 compare the percentage difference between the baseline profile and the profiles with the smallest amplitude. The baseline profile looses 60% of lift between $11<\alpha<16$ and experiences a 160% increase in drag over the same range of angles of attack. This performance is significantly worse than those obtained with the sinusoidal leading edge profiles. These profiles experienced a maximum loss of lift of 10% and a maximum gain in drag of 20% due to hysteresis. The performance of the aerofoils improved with a reduction in wavelength; however the improvement is less than 5% and can be considered to be negligible.

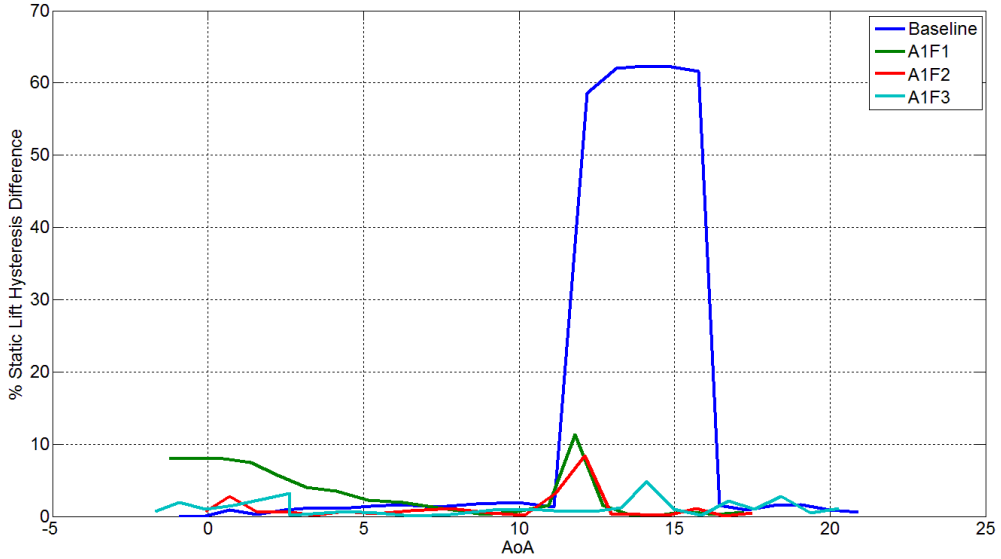

Figure 18: Percentage Lift coefficient hysteresis as a function of AoA for Baseline and Low Amplitude Aerofoils

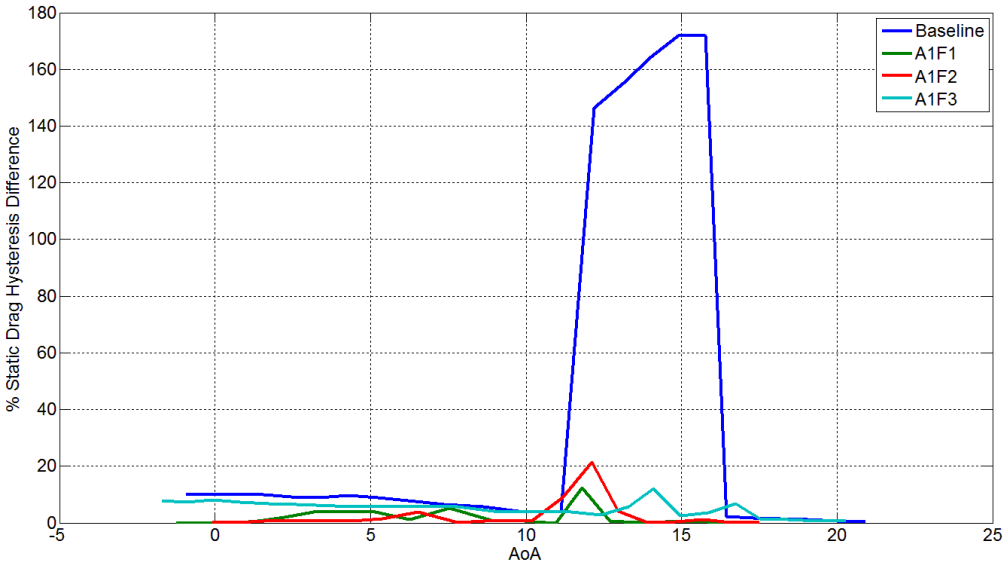

Figure 19: Percentage Drag coefficient hysteresis as a function of AoA for Baseline and Low Amplitude Aerofoils

The profiles with the larger amplitude exhibited a further improvement in performance with static lift and drag performance reductions of less than 8%. The effect of wavelength can also be considered to be insignificant for static hysteresis at the large amplitude.

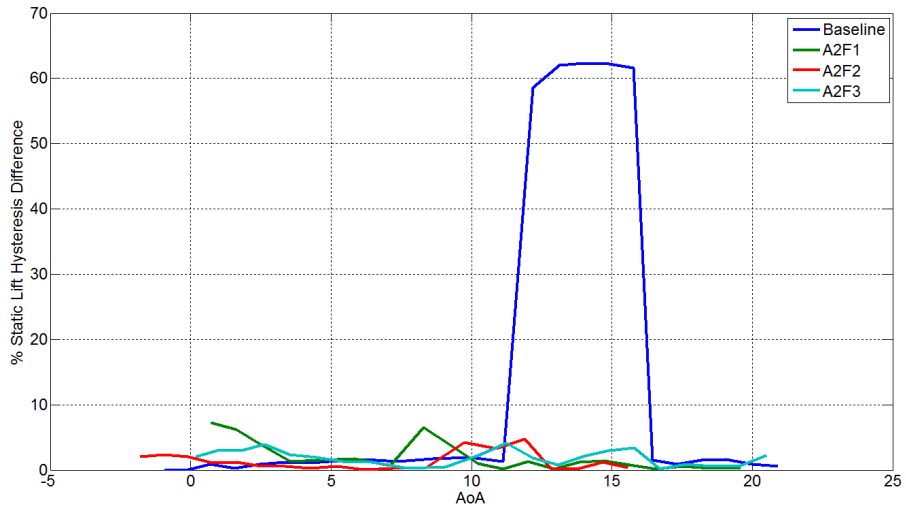

Figure 20: Percentage Lift coefficient hysteresis as a function of AoA for Baseline and High Amplitude Aerofoils

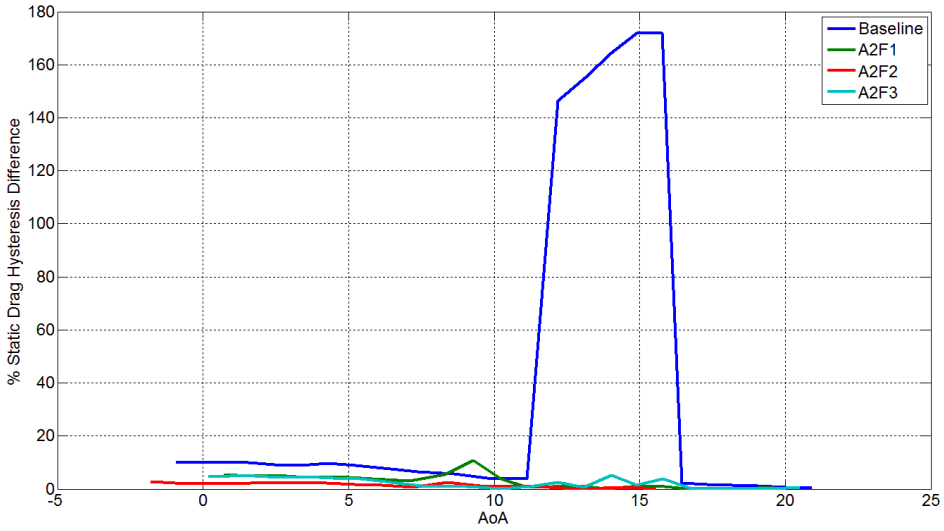

Figure 21: Percentage Drag coefficient hysteresis as a function of AoA for Baseline and High Amplitude Aerofoils

From the results presented above one can deduce that static hysteresis is significantly reduced for sinusoidal profiles with low amplitudes and practically nonexistent for aerofoils with large amplitudes. Thus, provided that the change in angle of attack is very small compared to the speed of the flow impinging the blade, the operational characteristics of an aerofoil with such leading edges can be considered to be constant over the whole operating range of angles of attack irrespective of the motion of the blade.

The complete set of hysteresis curves for all the profiles can be found in Appendix A.

3.3. Static Study Summary

3.3.1. Serrated Leading Edges Aerodynamic Analysis

The results from the static study corroborated with results from previous studies with respect to a number of features. The aerofoils having a large amplitude resulted in softer stall characteristics however they also displayed a significant reduction in the maximum lift coefficient. The aerofoils having the lower amplitude showed higher maximum lift coefficients both in pre-stall and post stall regions compared to the higher amplitude aerofoils. The maximum lift coefficient of the baseline aerofoil was not reached using the aerofoils with the sinusoidal leading edges. The latter aerofoils also resulted in lower drag coefficients compared to the high amplitude aerofoils. In all cases an increase in drag was recorded in the pre stall region, however in the post stall region there was negligible difference between the aerofoils and the baseline.

The results also showed that a reduction in wavelength resulted in an increase in the lift coefficient and stall angle. The stall behaviour was however found to be independent of wavelength with all three amplitudes resulting in the same percentage reduction of lift at stall at the same geometric amplitude.

The aerofoil with the best performance was found to be the one with the lowest amplitude and lowest wavelength. This aerofoil experienced a 35% reduction in lift in pre-stall, followed by an increase of 70% in post stall. The increase in drag was of 100% in pre-stall, followed by a negligible difference in post stall.

3.3.2. Static Hysteresis Analysis

The static hysteresis study revealed that the inclusion of peaks to the leading edge resulted in minimal to negligible hysteresis under static conditions. Whereas the baseline case experienced a 60% reduction in performance and a re-attachment angle of 5^0 lower than the stall angle, the aerofoils with the sinusoidal leading edges experienced a maximum of 10% hysteresis. The effect of wavelength was found to be negligible in this case. The performance of the aerofoils with the largest amplitudes was found to be marginally better than the aerofoils at the lowest amplitude.

Chapter 4. Results: Dynamic Stall

4.1. Introduction

The main objective of the dynamic study was to determine whether the sinusoidal leading edge profiles altered the performance of the baseline aerofoil in dynamic stall. To simulate dynamic stall the aerofoils were oscillated at a frequency of 5Hz about a mean angle of attack. Two mean angles of attack were selected for the analysis, one at an angle of approximately 3^0 less than the static stall angle and the other at approximately 5^0 above the static stall angle. The former angle was selected based on the previous work which was carried out on dynamic stall. At this angle and operation conditions, the aerofoils were expected to undergo deep dynamic stall, thus producing clear hysteresis loops.

The latter mean angle of attack was chosen based on the static performance of the sinusoidal leading edge aerofoils. Since the benefit of such aerofoils lies at high angles of attack under static conditions, the principle operating range of the aerofoils would be expected to be at such angles. Hence, should the aerofoil undergo unsteady flow, the resulting oscillations would occur at high angles of attack and it would therefore be beneficial to study the dynamic behaviour at such angles. The study also focussed on the effect of amplitude on the hysteresis loop.

4.2. Motion Control

The motion of the aerofoil was controlled through the LabView program described in Chapter 2. Due to the direct coupling of the motor and shaft, the aerofoil was oscillated by directly controlling the position of the motor. A 20 point sinusoidal profile was therefore fed to the motor controller at 0.01 second intervals per point and interpolated, resulting in the 5Hz sinusoidal motion of the motor.

Due to the time required to execute the built in interpolation function, as well as the torsional moments produced by the lift and drag forces on the aerofoil, the resulting motion was not purely sinusoidal. The figures below present two typical motions that were captured during the dynamic study. Figure 22 represents the sinusoidal motion typical for the baseline aerofoil, while Figure 23 represents the sinusoidal motions typical for the aerofoils with a sinusoidal leading edge. The general motion can be seen to be sinusoidal however, some overshoot was experienced in all cases. In some instances, the peaks of the oscillations were found to be distorted, resulting in a difference in the change of angle of attack between the purely sinusoidal motion and the actual motion of the aerofoils. The error between the two curves was however minimal in both cases and a good level of confidence in the final results can be assured.

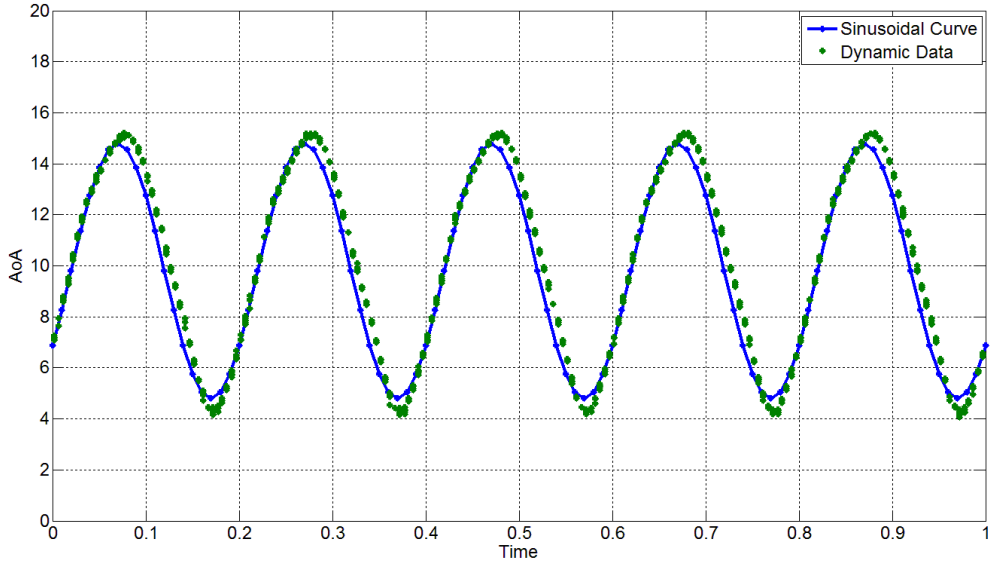

Figure 22: Pure Sinusoidal Profile superimposed on typical Baseline Aerofoil motion

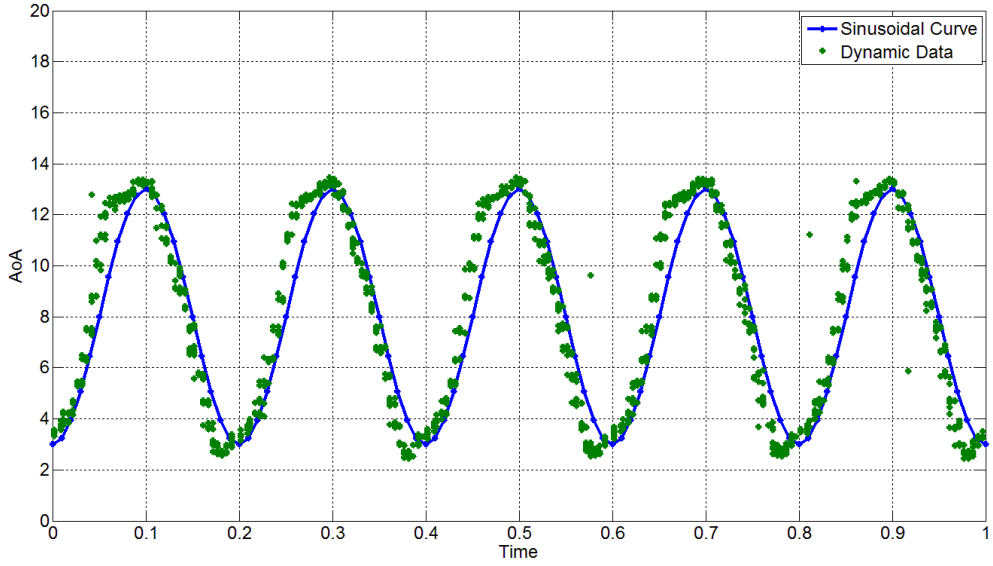

Figure 23: Pure Sinusoidal Profile superimposed on typical sinusoidal leading edge Aerofoil motion

4.3. Baseline Aerofoil analysis

Figure 24 below shows the dynamic stall results for the baseline aerofoil at a mean angle of attack of 13^0 and two amplitudes of 5^0 and 7^0. The shape of the loops indicates that using these operating conditions deep dynamic stall was achieved, with the characteristic features of dynamic stall being clearly identifiable. A significant increase in lift was recorded on the pitch up motion of the aerofoil with the maximum C_l reaching 1.2 for an amplitude of 5^0, and 1.4 for an amplitude of 7^0. These translate to an increase of 33% and 53% in the maximum lift coefficient for the low and high amplitude oscillations respectively. As expected, this increase was followed by a drastic reduction in lift until the flow reattached at the lowest point of the loop. The loss of lift for the low and high amplitude oscillations were of 0.7 and 0.9 respectively which represent 86% and 100% of the maximum static lift coefficient. These values highlight the need to control dynamic stall since such a drastic variation in lift limits the fatigue life of the shaft supporting the blade significantly, as well as increasing the cost of maintenance of such structures.

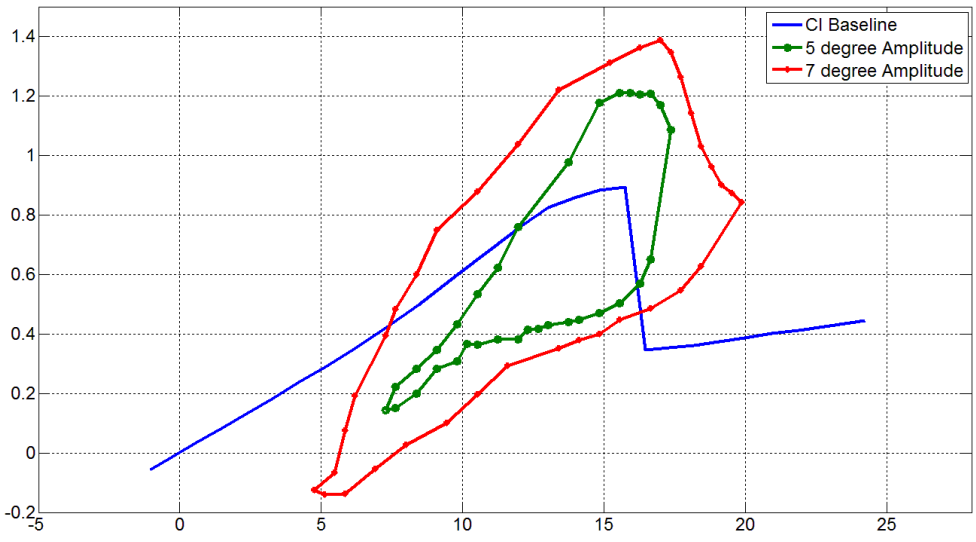

Figure 24: Dynamic Stall of Baseline Profile at $\alpha_0 = 13^0$ $\alpha_m = 5^0$ and $\alpha_m = 7^0$ at k=0.08

4.4. Sinusoidal Leading Edge Analysis

The complete results for the sinusoidal leading edges showing the hysteresis loops at the two median angles of attack and amplitudes are presented in Appendix B. The results presented below in Figure 25 to Figure 27 show the difference in C_l over the range of angles of attack of each aerofoil under dynamic motion.

Figure 25 and Figure 26 compare the difference in Cl when the aerofoils were oscillated about a mean angle of attack that was approximately 3 degrees lower than the static stall angle of that aerofoil, at amplitudes of 5^0 and 7^0 respectively. The results show that for the baseline aerofoil the difference grows with increasing angle of attack forming the loop seen in Figure 24 above. The aerofoils with a sinusoidal leading edge however show a different tendency to produce a hysteresis curve which is altogether different than that achieved for the baseline case. Whilst for low angles of attack, within the operational envelope, the difference in Cl increases with increasing angle of attack, at a point the difference reaches a saturation point and the remains virtually constant for the rest of the angles. The difference is also significantly lower than the baseline case with a maximum difference of 0.3 compared to the 0.7 difference for the baseline case at the lowest amplitude of oscillation. Similarly at the highest amplitude the maximum difference in the hysteresis loop was 0.5 for the sinusoidal leading edge profiles, compared to 0.9 for the baseline case.

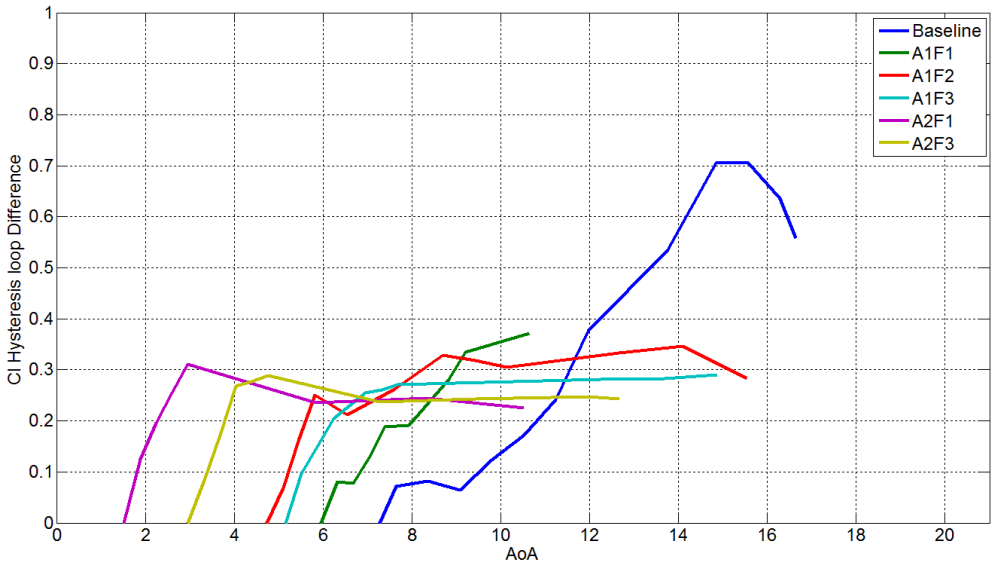

Figure 25: Lift Coefficient Hysteresis Loop Difference at $\alpha_m = 5^0$, $\alpha_0 = \alpha_{stall} - 3^0$, k=0.08

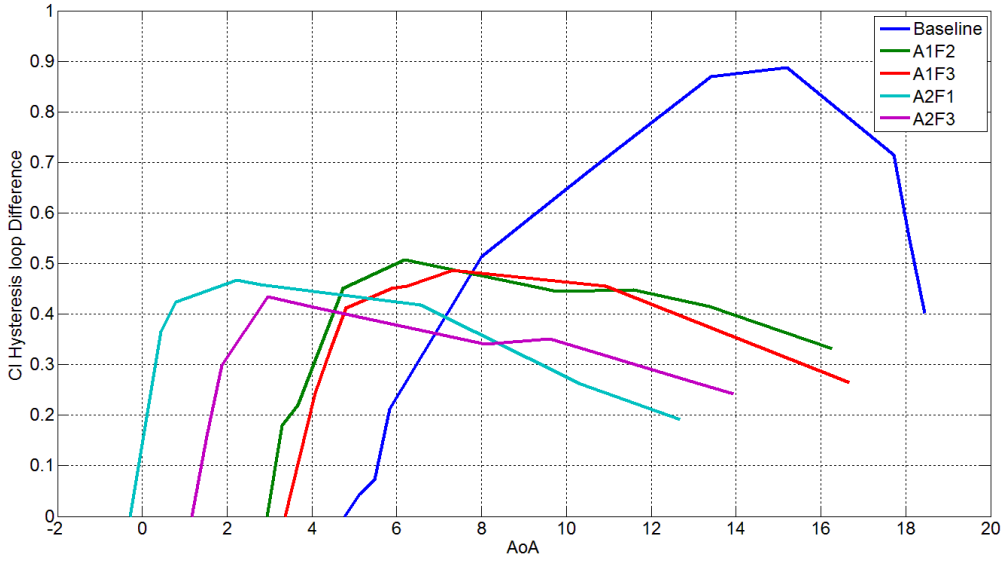

Figure 26: Lift Coefficient Hysteresis Loop Difference at α_m =7⁰, $\alpha_0 = \alpha_0 - 3^0$, k=0.08

The results show that the maximum difference in lift experienced by each aerofoil is 60%, 52%, 39% of the maximum lift at the lowest geometrical amplitude at successively lower distances between peaks. The resulting increase in maximum lift is 55%, 37%, 26% of the static maximum Cl for the same aerofoils respectively. This shows that the aerofoils with the low geometrical amplitude produce more lift and also experience a lower lift difference than the baseline case. The aerofoil with the largest spacing between peaks produces the most lift but also experiences the largest hysteresis. The aerofoil with the lowest distance between peaks on the other hand produces less lift but experiences lower hysteresis. Generating 52% more lift and experiencing 37% hysteresis the aerofoil with medium spacing between peaks offers a compromise between the other two geometries.

At the largest geometrical amplitude, the maximum lift generated by the aerofoils was 42% and 44% higher for the aerofoils with the largest and smallest distance between peaks respectively. These aerofoils also experienced a hysteresis difference in lift of 61% and 63% respectively. The effect of geometrical wavelength was not evident in this case with both the large and small wavelength resulting in similar results.

Both sets of aerofoils having different geometrical amplitudes showed an improved performance over the baseline aerofoil, however the aerofoils having the lowest geometrical amplitude performed better with respect to both the maximum lift generated and hysteresis.

The results at the second mean angle of attack in Figure 27 however show no improvement over the baseline case. The sinusoidal leading edge profiles actually performed slightly worse than the baseline aerofoil with an increase of 0.5 in the lift coefficient hysteresis loop for all aerofoils. The difference between the different profiles was also negligible. The sinusoidal leading edge profiles offer no advantage for dynamic stall at angles of attack beyond the static stall angle.

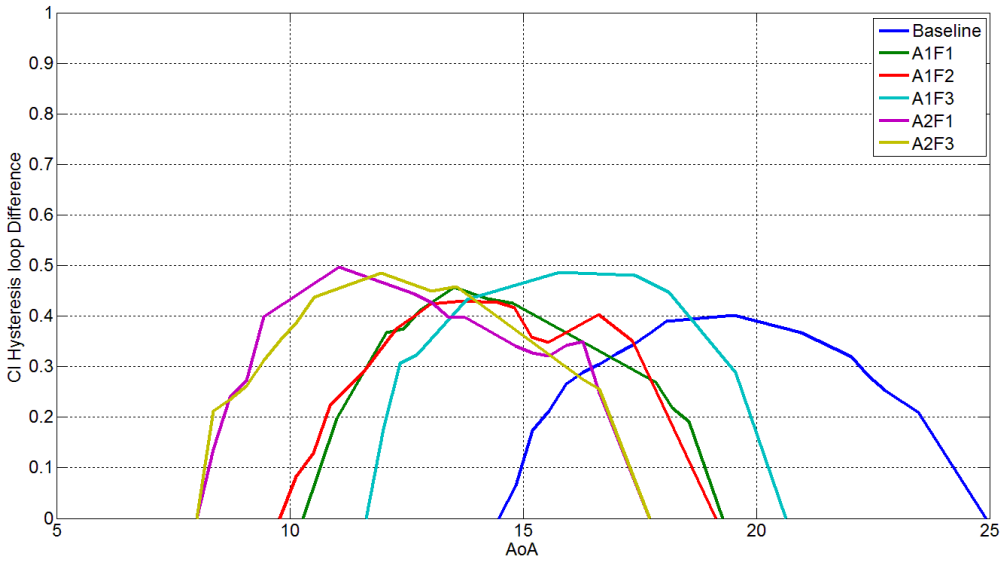

Figure 27: Lift Coefficient Hysteresis Loop Difference at α_m =7⁰, $\alpha_0 = \alpha_0 + 5^0$, k=0.08

4.5. Dynamic stall study Summary

The dynamic stall study revealed that the inclusion of the sinusoidal leading edges led to a significant improvement over the results from the baseline aerofoil with an increase in the maximum lift generated as well as less hysteresis. At a mean angle of approximately 3^0 less than the static stall angle for each aerofoil and at an amplitude of 5^0 at a reduced frequency of k=0.08, the baseline aerofoil produced 33% more lift followed by a drop of 86% of the maximum static stall lift.

The results from the sinusoidal leading edge aerofoils showed that both the maximum lift coefficient and hysteresis increase with increasing spacing between peaks at the lowest geometrical amplitude. At the largest geometrical amplitude the effect of peak spacing was not so pronounced.

At an angle of attack of approximately 5^0 higher than the static stall angle the sinusoidal leading edge profiles offered no advantage in performance compared to the baseline case.

The best overall performance in terms of hysteresis reduction was achieved with the aerofoil having the lowest amplitude and shortest distance between peaks with a 26% increase in maximum lift coefficient and 39% hysteresis.

Chapter 5. Conclusions and Further Work

5.1. Conclusion

Clearly the advantage of using a sinusoidal leading edge profile is dependent upon the particular application of use. If the main aim in the engineering system is to get the highest possible lift, then based on the results obtained, using a sinusoidal leading edge at low Reynolds numbers is clearly not a solution. It is as yet unclear whether an increase in Reynolds number to high values in the range of 10^6 will increase the maximum lift coefficient to a value higher than the baseline aerofoil.

The main advantage of using these leading edges lies in applications where the principle operating range is at high angles of attack, close to the static stall angle, and in unsteady flow conditions. The static hysteresis performance is particularly beneficial when the angle of attack is changing slowly relative to the oncoming flow. The aerofoil leading edges are however also beneficial in applications with rapidly changing angles of attack due to the lower levels of hysteresis as well as an increase in the maximum lift coefficient.

Optimisation of the geometrical amplitude and wavelength is required depending on the application however these investigations indicate that the low amplitude and short wavelength aerofoils offer superior performance over the other configurations under most operating conditions.

5.2. Further Work

- Extensive dynamic stall experiments together with flow visualisation have been carried out to determine how the flow develops over the aerofoil to produce the hysteresis loop. Since the leading edge geometry has been shown to produce contra rotating vortices, it would be interesting to understand how the flow develops over the aerofoil under dynamic stall by applying pressure taps to the aerofoil and by conducting PIV experiments.

- The centrifugal forces experienced by the flow on a rotating blade push the air radially outward suppressing separation and hence increasing the lift generated by the blade as well as delaying stall to higher angles of attack. Wind turbines benefit from the stall delay phenomenon to produce greater lift than that predicted in static tests. Wind turbines however also experience dynamic stall due to the constant change in wind direction and the resulting misalignment of the turbine axis to wind direction (Yaw Error).

  Previous studies have indicated that the accelerated flow caused by the peaks act as wing fences, reducing span-wise flow. This could prove to be detrimental to the wind turbine's performance; however, this study has also revealed that the operation of an aerofoil in dynamic stall is improved by using such a leading edge. A study into the three dimensional performance of a rotating blade would be beneficial to determine if the benefit of reducing dynamic stall outweighs the improvement caused by the span-wise flow.

- The generation of noise from wind turbines, particularly wing tip noise, is of concern when wind turbines are installed close to residential areas. A further investigation could also be carried out to determine whether the sinusoidal leading edge can be applied to the tip of a wind turbine blade to reduce this noise.

References

[1] J. G. Leishman, Principles of Helicopter Aerodynamics, New York: Cambridge University Press, 2006.

[2] F. E. Fish, P. W. Weber, M. M. Murray and L. E. Howle, "The Tubercles on Humpback Whales' Flippers: Application of Bio-Inspired Technology," *Integrative and Comparative Biology,* vol. 51, no. 1, pp. 203-213, 2011.

[3] F. E. Fish, "Biomimetics: Determining engineering opportunities from nature," *Proceedings SPIE Conference,* vol. 7401, no. 740109-1.

[4] "National Geographic," [Online]. Available: http://animals.nationalgeographic.com/animals/mammals/humpback-whale/. [Accessed 29th March 2012].

[5] B. L. Woodward, F. E. Fish and J. P. Winn, "Morphological Specializations of Baleen Whales Associated With Hydrodynamic Performance and Ecological Niche," *Journal of Morphology,* vol. 267, pp. 1284-1294, 2006.

[6] F. Fish and J. Battle, "Hydrodynamic Design of the Humpback Whale Flipper," *Journal of Morphology,* vol. 225, pp. 51-60, 1995.

[7] D. Miklosovic, M. Murray, L. Howle and F. Fish, "Leading-edge tubercles delay stall on humpback whale (Megaptera novaeangliae) flippers," *Physics of Fluids,* vol. 16, no. 5, pp. L39-42, 2004.

[8] D. S. Miklosovic and M. M. Murray, "Experimental Evaluation of Sinusoidal Leading Edges," *Journal of Aircraft,* vol. 44, no. 4, pp. 1404-1407, 2007.

[9] H. Johari, C. Henoch, D. Cusodio and A. Levshin, "Effects of Leading-Edge Protuberances on Airfoil Performance," *AIAA Journal,* vol. 45, no. 11, pp. 2634-2642, 2007.

[10] K. L. Hansen, R. M. Kelso and B. B. Dally, "An Investigation of Three-Dimensional Effects on the Performance of Tubercles at Low Reynolds Numbers," in *17th Australian Fluid Mechanics Conference*, Auckland, New Zealand, 2010.

[11] K. L. Hansen, R. M. Kelso and B. B. Dally, "Performance Variations of Leading-Edge Tubercles for Distinct Airfoil Profiles," *AIAA Journal,* vol. 49, no. 1, pp. 185-194, 2011.

[12] J. D. Anderson, Fundamentals of Aerodynamics, NewYork: McGraw Hill, 2001.

[13] E. van Nierop, S. Alben and M. P. Brenner, “How Bumps on Whale Flippers Delay Stall: An Aerodynamic Model,” *Physics Review Letters,* vol. 100, no. 054502, 2008.

[14] M. J. Stanway, “Hydrodynamic effects of Leading-Edge tubercles on control surfaces and in flapping foil propulsion,” Massachusetts Institute of Technology, M.S. Thesis, 2008.

[15] W. McCroskey, “The Phenomenon of Dynamic Stall,” NASA TM-81264, 1981.

[16] J. G. Leishman and T. S. Beddoes, “A Semi-Empirical Model for Dynamic Stall,” *Journal of American Helicopter Society,* vol. 34, no. 3, pp. 3-17, 1989.

[17] B. E. Brydges, “Flow Visualization of Dynamic Stall on an Oscillating Airfoil,” Naval Postgraduate School, Monterey, California, Thesis, 1989.

[18] J. G. Leishman, “Dynamic Stall Experiments on the NACA 23012 aerofoil,” *Experiments in Fluids,* vol. 9, pp. 49-59, 1990.

[19] C. A. Ozen and D. Rockwell, “Control of vortical structures on a flapping wing via a sinusoidal leading-edge,” *Physics of Fluids,* vol. 22, no. 021701, 2010.

[20] B. Heine, K. Mulleners, A. Gardner and H. Mai, “On the effects of leading Edge Vortex Generators on an OA209 Airfoil,” in *ODAS2009*, 2009.

[21] P. Watts and F. E. Fish, “The Influence of Passive, Leading Edge Tubercles on Wing Performance,” in *Proc. of Unmanned Untethered Submersibe Tech. (UUST)*, Durnham, 2001.

[22] B. E. Brydges, “Flow Visualization of Dynamic Stall on an Oscillatin Airfoil,” Naval Postgraduate School, Monterey, California, Thesis, 1989.

Appendix A

Static Hysteresis Figures

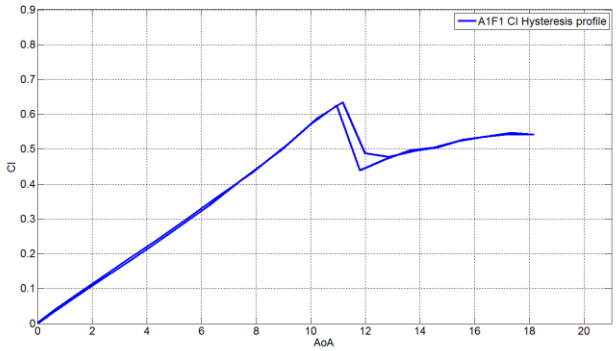

Figure 28: Static Lift Coefficient Hysteresis data for A1F1 Profile

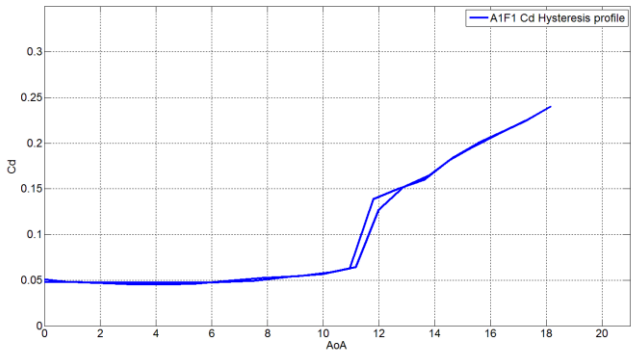

Figure 29: Static Drag Coefficient Hysteresis data for A1F1 Profile

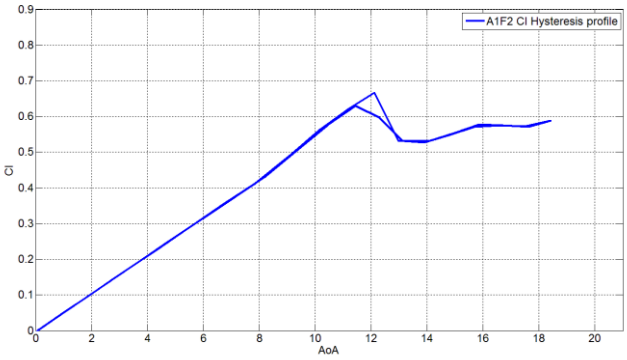

Figure 30: Static Lift Coefficient Hysteresis data for A1F2 Profile

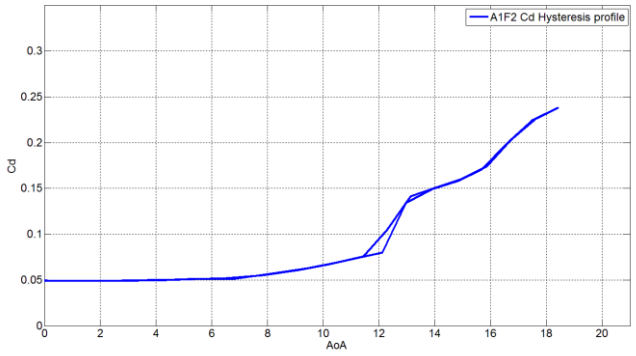

Figure 31: Static Drag Coefficient Hysteresis data for A1F2 Profile

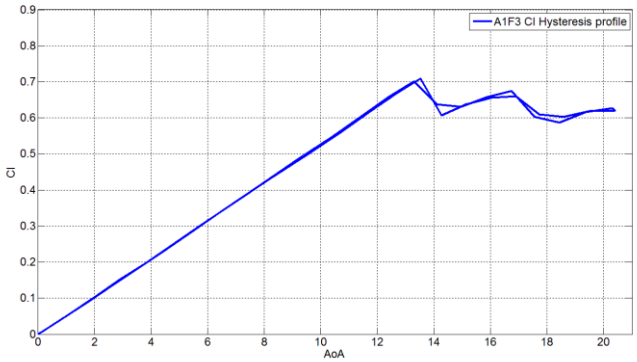

Figure 32: Static Lift Coefficient Hysteresis data for A1F3 Profile

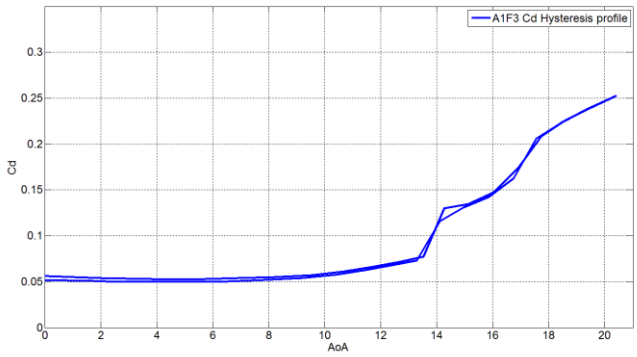

Figure 33: Static Drag Coefficient Hysteresis data for A1F3 Profile

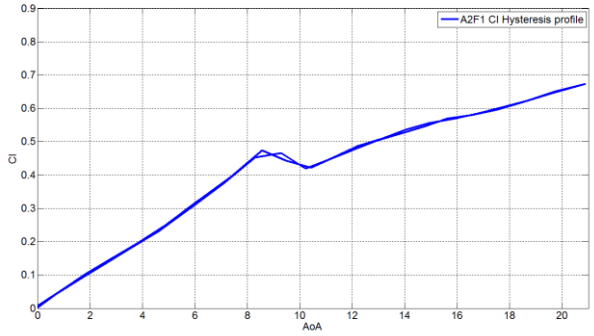

Figure 34: Static Lift Coefficient Hysteresis data for A2F1 Profile

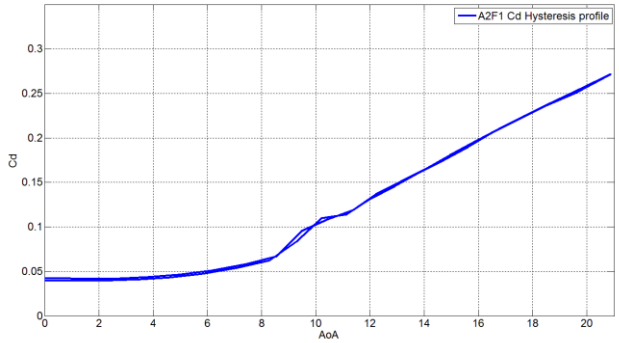

Figure 35: Static Drag Coefficient Hysteresis data for A2F1 Profile

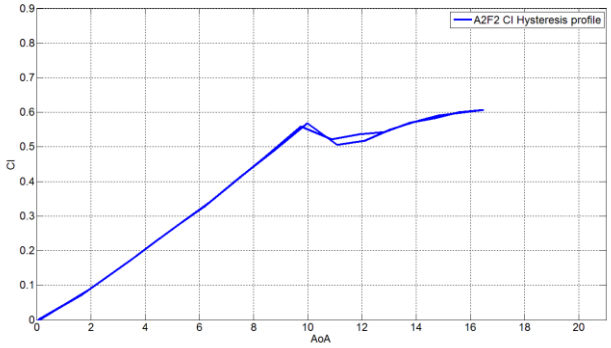

Figure 36: Static Lift Coefficient Hysteresis data for A2F2 Profile

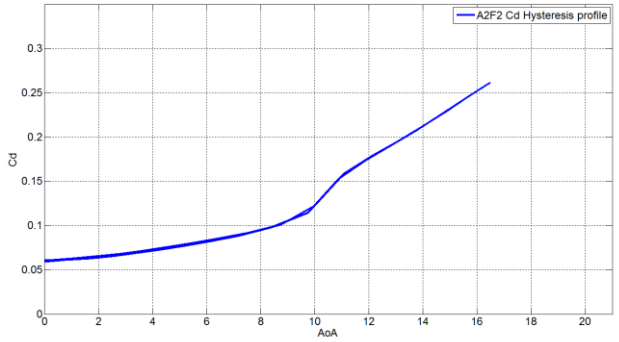

Figure 37: Static Drag Coefficient Hysteresis data for A2F2 Profile

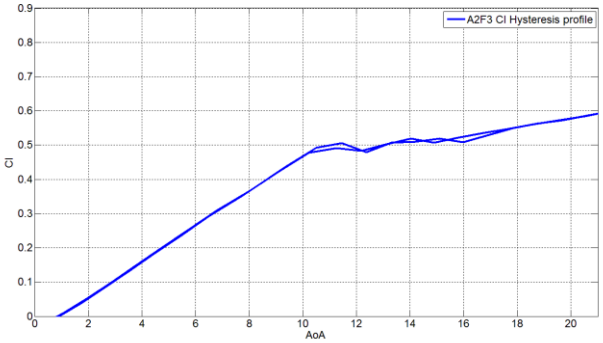

Figure 38: Static Lift Coefficient Hysteresis data for A2F3 Profile

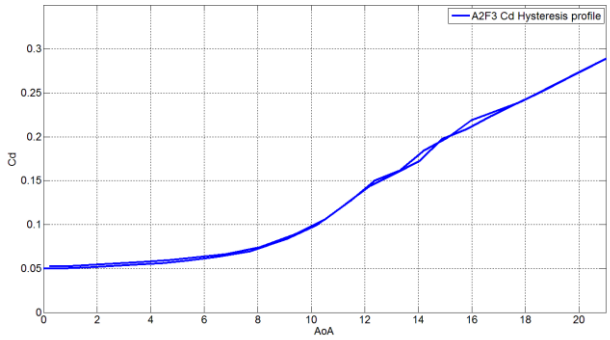

Figure 39: Static Drag Coefficient Hysteresis data for A2F3 Profile

Appendix B

Dynamic Stall Results At $\alpha_m = \alpha_{stall} - 3^0$, k=0.08

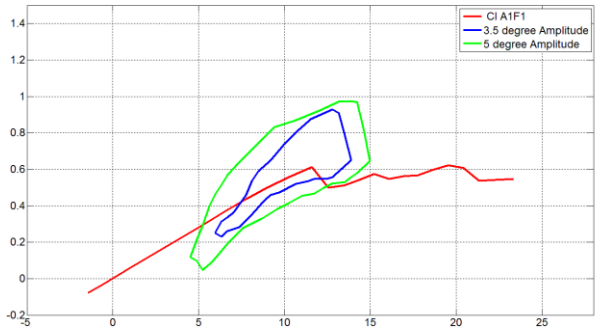

Figure 40: A1F1 Hysteresis loop

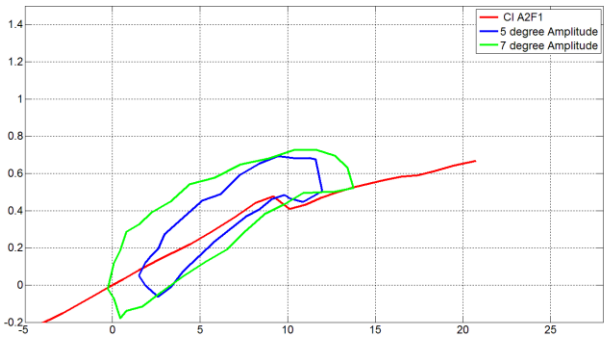

Figure 41: A2F1 Hysteresis loop

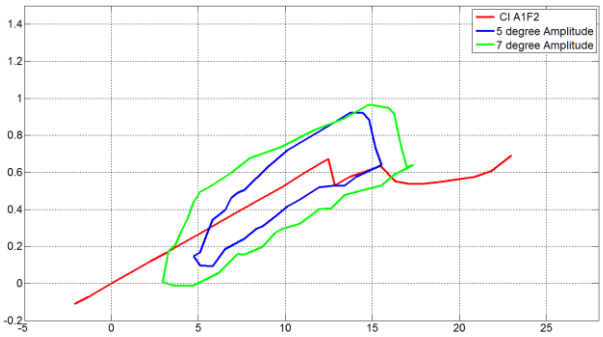

Figure 42: A1F2 Hysteresis loop

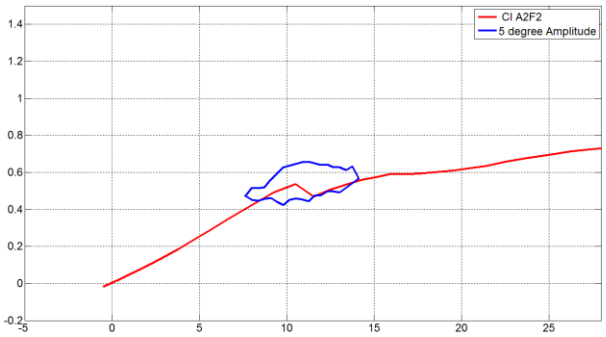

Figure 43: A2F2 Hysteresis loop

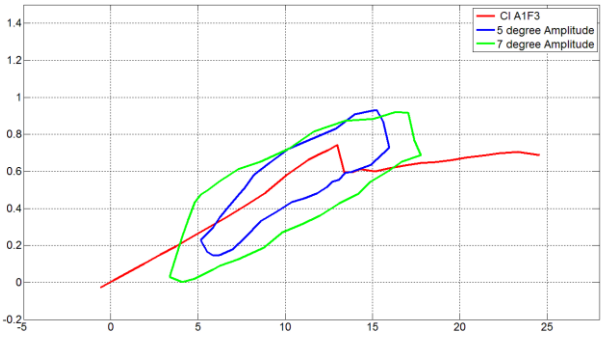

Figure 44: A1F3 Hysteresis loop

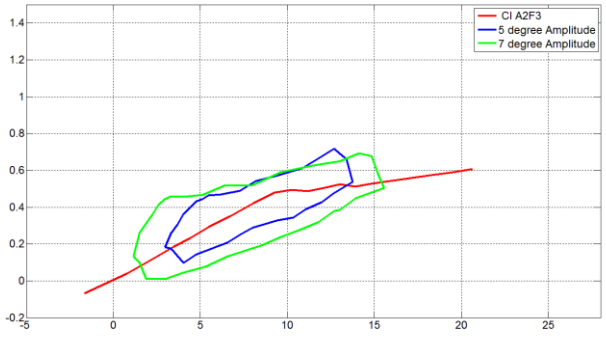

Figure 45: A2F3 Hysteresis loop

At $\alpha_m = \alpha_{stall} + 5^0$, k=0.08

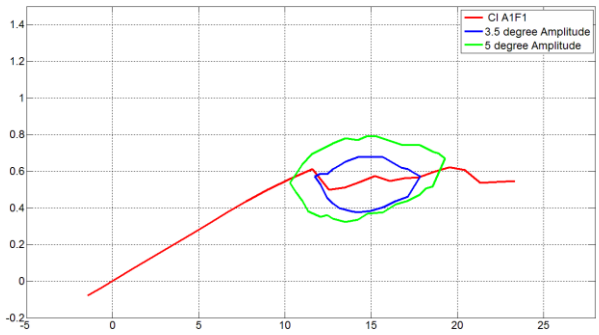

Figure 46: A1F1 Hysteresis loop

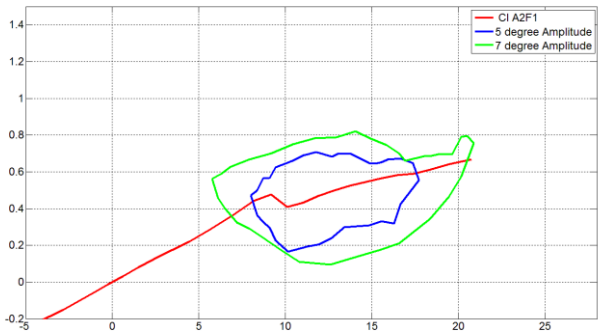

Figure 47: A2F1 Hysteresis loop

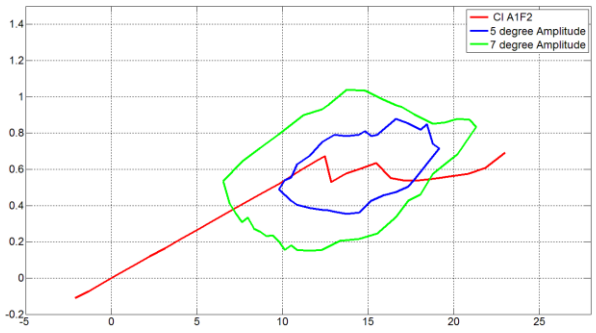

Figure 48: A1F2 Hysteresis loop

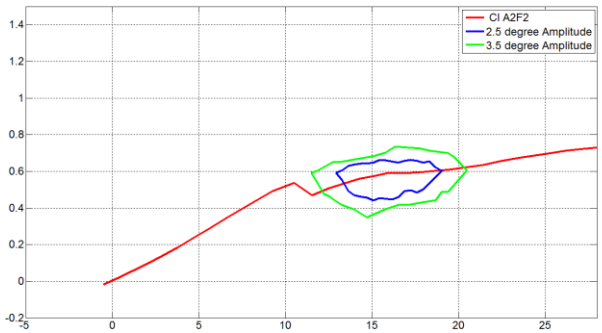

Figure 49: A2F2 Hysteresis loop

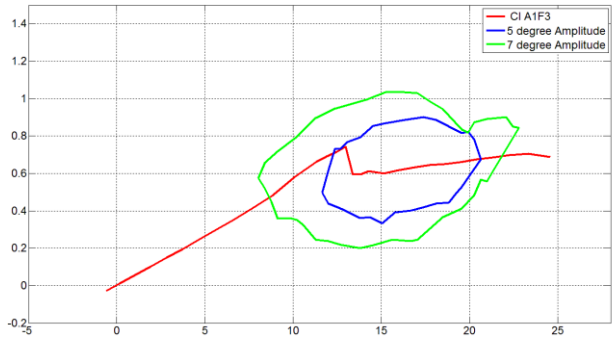

Figure 50: A1F3 Hysteresis loop

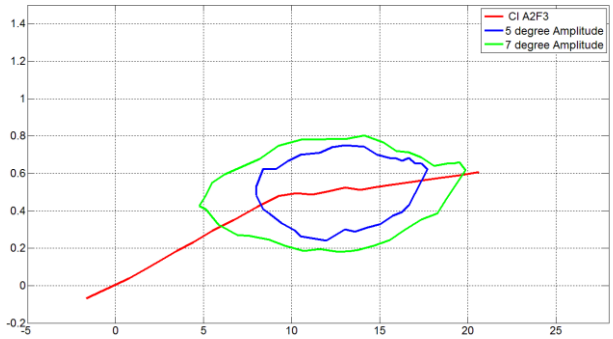

Figure 51: A2F3 Hysteresis loop

Appendix C

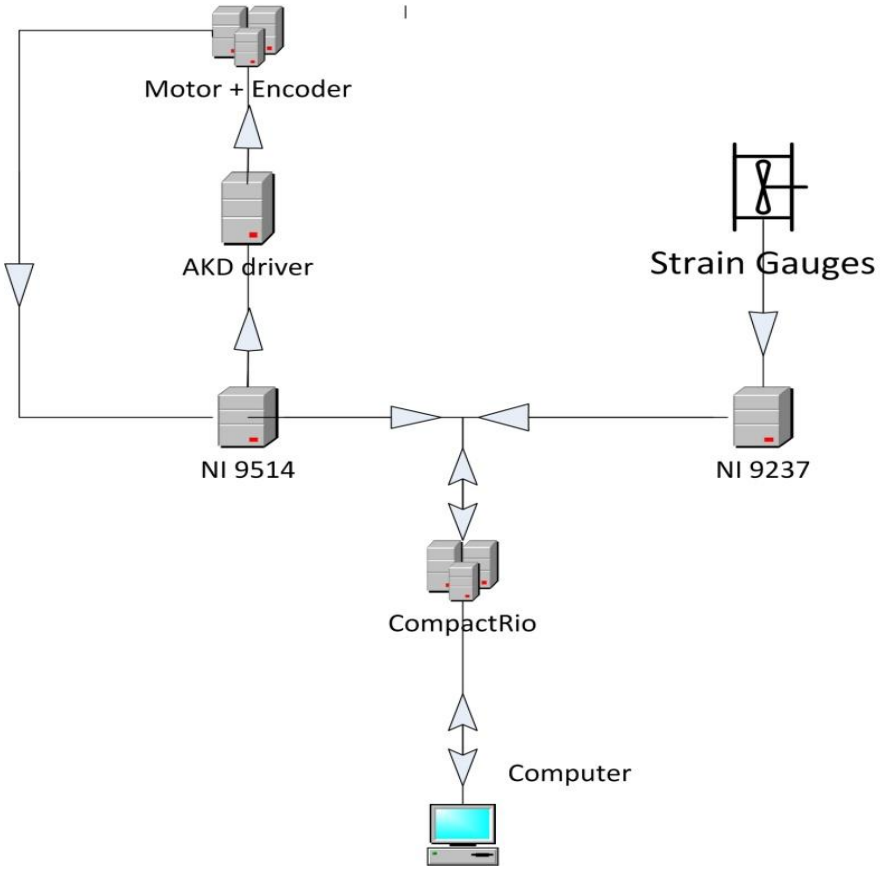

Figure 52: Data Flow Diagram